HTGL

Tunable Diode Laser Sensors to Monitor Temperature and Gas Composition in High-Temperature Coal Gasifiers

DE-FE0001180

Final Scientific/Technical Report
Reporting Period: Oct 1, 2009-Sept 30, 2014

Professor Ronald K. Hanson, PI

December 2014

High Temperature Gasdynamics Laboratory
Mechanical Engineering Department
Stanford University, Stanford CA 94305

Subcontractor
Professor Kevin J. Whitty
Department of Chemical Engineering, Institute for Clean and Secure Energy (ICSE), University of Utah, Salt Lake City, Utah

Disclaimer

Abstract

The integrated gasification combined cycle (IGCC) when combined with carbon capture and storage can be one of the cleanest methods of extracting energy from coal. Control of coal and biomass gasification processes to accommodate the changing character of input-fuel streams is required for practical implementation of integrated gasification combined-cycle (IGCC) technologies. Therefore a fast time-response sensor is needed for real-time monitoring of the composition and ideally the heating value of the synthesis gas (here called syngas) as it exits the gasifier. The goal of this project was the design, construction, and demonstration an *in situ* laser-absorption sensor to monitor multiple species in the syngas output from practical-scale coal gasifiers. This project investigated the hypothesis of using laser absorption sensing in particulate-laden syngas. Absorption transitions were selected with design rules to optimize signal strength while minimizing interference from other species. Successful *in situ* measurements in the dusty, high-pressure syngas flow were enabled by Stanford's normalized and scanned wavelength modulation strategy. A prototype sensor for CO, CH_4, CO_2, and H_2O was refined with experiments conducted in the laboratory at Stanford University, a pilot-scale at the University of Utah, and an engineering-scale gasifier at DoE's National Center for Carbon Capture with the demonstration of a prototype sensor with technical readiness level 6 in the 2014 measurement campaign.

Table of Contents

Executive Summary

Extraction of energy from coal combustion results in the emission of greenhouse gases such as CO_2 and CH_4 and other environmentally hazardous gases including CO, SO_2, H_2S and NO_x. Public awareness and legislation have led to goals for the worldwide reduction of greenhouse gas and other harmful gas emissions. However, coal remains the most widely used fuel for the generation of electricity, and efforts to reduce emissions from coal combustion could have important societal impact. Integrated gasification combined cycle (IGCC) when combined with carbon and sulfur sequestration and storage can be one of the cleanest methods of extraction of energy from coal. To effectively operate and control the performance and the output power from an IGCC system, the heating value of the synthesis gas output from the gasifier must be properly matched with the air intake of the gas turbine. Because of the variable energy content of the coal feedstock and the sensitive variation of the syngas composition with gasifier reactor conditions, a fast monitor of the output syngas is needed as a control sensor for optimum system performance. Conventionally, extractive sampling and gas chromatographic analysis can be used for syngas analysis. However, often the sample extraction and preparation (depressurization, cooling, dehumidification and filtration of particulates) significantly degrades the time response and a faster control variable is required for gasifier control. Solution of this syngas analysis problem has been recognized as a crucial requirement for the improvement of control and instrumentation of gasifiers by the U.S. Department of Energy [1].

The research reported here focuses on investigation of the hypothesis that *in situ* laser absorption of the output syngas from a coal gasifier could provide the gas composition monitor with the needed time response for a gasifier control sensor. *In situ* syngas measurements present two formidable challenges to laser absorption sensing. First, the high pressure needed for efficient coal gasification broadens and blends the absorption spectra of the syngas components, reducing the peak signals and increasing the difficulty species selective measurements due to interference absorption by other species in the syngas. Second, the particulate loading in syngas produces large time-varying non-absorption losses of the laser transmission making quantitative determination of the absorption contribution to the transmission loss quite difficult. Over the past decade Stanford University has been developing a wavelength-scanned, normalized, wavelength modulation spectroscopy (WMS) strategy for harsh, reactive, combustion gas environments. The research here investigates the application of this laser absorption measurement scheme to *in situ* monitoring of multiple species in the product syngas flow from industrial-scale coal gasifiers.

The research conducted on this project included four distinct activities: (1) sensor design, (2) laboratory validation of sensor performance, (3) field measurements in a pilot-scale research gasifier, and (4) field measurements in an engineering-scale coal gasifier. During each of these phases, the fabrication of the prototype sensor was optimized to incorporate the lessons learned in the prior application experiments. This project focused on the measurements of CO, CO_2, CH_4 and H_2O in syngas.

(1) Sensor design was done with spectral simulations conducted using published spectral databases for these molecules augmented with Stanford measurements of spectral constants using laser absorption of pure and mixed gases in heated cells. These calculations enabled the selection of candidate sensor wavelengths for each species that would allow sensitive measurements while minimizing interference absorption from other species. A method to calculate heating value (and Wobbe Index) using the four species measurements was developed that provided accurate results

for oxygen-blown gasifiers. The research partially supported the invention of a unique method to interpret wavelength-scanned, normalized-WMS data, which provided a new scheme for accurate WMS measurements in reactive gas flows with unknown composition.

(2) Laboratory validation of the sensor performance was performed using lasers tuned to the candidate wavelengths selected in the first phase, and a first-generation prototype sensor was then assembled and tested in the laboratory at Stanford. The sensor performance was evaluated using gas mixtures in heated and pressurized gas cells, and compared with predicted performance to validate the spectral model calculations. These experiments were used to finalize the sensor wavelength selection and optimized laser modulation parameters for CO, CO_2, CH_4, and H_2O at 600K and pressures up to 30 atm.

(3) Four field measurement campaigns were then conducted in the syngas products of the pilot-scale coal gasifier at the University of Utah (August 2010, December 2010, August 2011, and June 2012). These field campaigns included a significant optical engineering task. The development of optical access for *in situ* laser absorption in the syngas flow was an important part of this work. The lessons learned during each campaign were used to refine the sensor, and the sensor performance improved for each campaign. The June 2012 campaign included successful time-resolved measurements of CO, CO_2, CH_4 and H_2O for gasifier operation periods exceeding ten hours.

(4) Two field measurement campaigns to monitor the syngas output from the engineering-scale transport gasifier at the National Center for Carbon Capture (NCCC) in Wilsonville, AL were conducted. The first campaign in November/December 2012 tested the optical access and monitored H_2O during run R09. That measurement campaign was the first ever laser absorption application at the NCCC facility and a significant part of the research involved developing a safe optical access for use in the commercial environment of the NCCC gasifier. The second campaign used the four species CO, CO_2, CH_4, and H_2O sensor optimized in the Utah gasifier for measurements in the syngas during run R13 conducted in March and April, 2014. The measurements were in good agreement with gas chromatography (GC) analysis of samples, but the *in situ* laser sensor had much faster time response, ~1 second compared with the 20 minute delay and 15 minute response of the GC analysis due to transit time and gas diffusion in the filters and driers in the sampling line. The time response of the *in situ* laser absorption and the rapid transport of the syngas products enabled gasifier reactor dynamics to be observed at the measurement location downstream of the particulate control device. The demonstration measurement shows the *in situ* laser absorption sensor has the time response needed for reactor control. The NCCC measurement campaign demonstrated a technical readiness level of 6, and we anticipate only one more year of development would be needed to bring this multi-species laser absorption sensor for coal gasification (and other particulate-laden applications) to a technical readiness level of 7 or possibly 8; thus, we suggest this sensor presents an opportunity for future DoE investment.

All of the milestones identified in the original and supplemental proposals have been completed, and the results have been published in the peer-reviewed literature.

Report Details

This research project sought to develop laser absorption sensing for coal gasification and a successful demonstration was performed of a four-color sensor for simultaneous *in situ* measurements of CO, CO_2, CH_4, and H_2O in the synthesis gas products from large-scale coal gasifiers. The work included four distinct activities: (1) sensor design, (2) laboratory validation of sensor performance, (3) field measurements in a pilot-scale research gasifier, and (4) field measurements in an engineering-scale coal gasifier, which will be discussed in the sections below. The sensor prototype designed in section 1 and tested in section 2 was continually improved and refined to address the lessons learned during each set of experiments.

1. Sensor design

1.1 Absorption spectroscopy and line selection

The laser absorption sensor concept investigated here is illustrated in the cartoon of Fig. 1, which shows a set of *n* fiber-coupled diode lasers multiplexed onto a common measurement path.

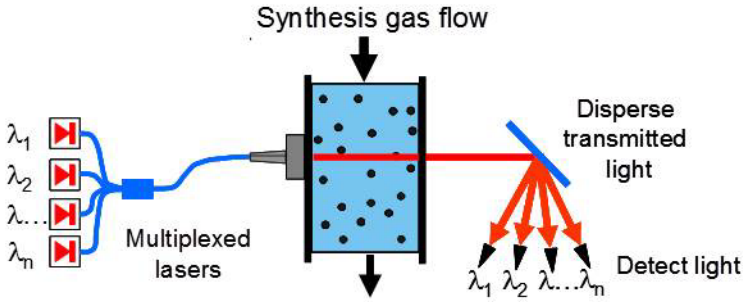

Figure 1: Wavelength-multiplexed multi-species absorption sensor.

The light is then directed across the syngas product duct and the transmitted light from each laser is independently detected. The mole fraction of each of the n species can then be determined from the Beer-Lambert law:

$$\tau(\nu) = \frac{I}{I_0} = e^{-\alpha(\nu)}$$

where I_0 is the incident beam intensity, I is the transmitted beam intensity, ν is the frequency of the monochromatic laser light, and α is the spectral absorbance:

$$\alpha(\nu) = P \cdot L \cdot \sum_{i,j} x_i \cdot S_{i,j} \cdot \phi_{i,j}(\nu)$$

where P is the gas pressure, L the path length L, x_i the mole fraction of the i^{th} absorbing species, $S_{i,j}$ the transition linestrength and $\phi_{ij}(\nu)$ the lineshape function of the j^{th} transition assuming a uniform gas composition and temperature along the laser line of sight (LOS). For an isolated transition, the total area integrating the absorbance by scanning the laser wavelength simplifies and becomes

$$\int_{-\infty}^{\infty} \alpha(\nu) d\nu = P \cdot x_i \cdot L \cdot S_{i,j}$$

The first step in the design of an *in situ* laser absorption sensor was the evaluation of the absorption spectra of the chemical species expected in the target gas at a relevant temperature and

pressure. Here we considered the primary products of oxygen-blown, low-sulfur coal gasification: H_2, CO, CO_2, H_2O and CH_4. As a homonuclear diatomic molecule, H_2 does not have infrared active absorption transitions, and thus the sensor described in this research did not monitor H_2 directly. Later in this section we will discuss determination of the H_2 mole fraction from a gas balance calculation. For high sulfur coal, SO_2 must also be monitored, which could be accomplished by adding another wavelength into our multi-color, multi-species sensor strategy. Similarly for an air-blown gasifier, NH_3 must also be considered, and again measurement of NH_3 only would require the addition of another channel to our multi-species concept.

The initial data needed for the four-species sensor investigated here were the survey absorption spectra shown in Fig. 2, which is an overlay for the near-infrared absorption at 15 atm pressure and 600 K for a 20 cm path length in the target gas for 10% H_2O in air, 10% CO_2 in air, 10% CO in air, and 1% CH_4 in air. These data showed that detection of the overtone and combination bands of H_2O in the region around 1400 and 1900 nm offer many possible transitions that are free from any interference absorption of the other components in the syngas. CO and CO_2 are severely limited by the predicted H_2O interference, and although the best candidates were selected based on the simulation calculation, spectroscopic measurements in heated cells were required to validate the data.

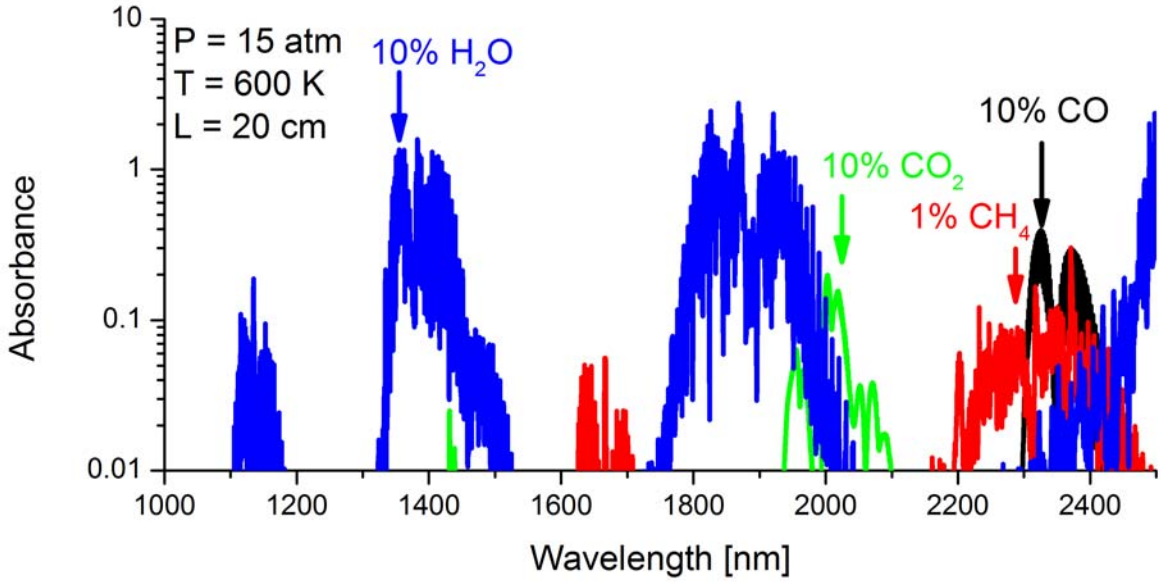

Figure 2: Absorption spectra calculated for 600 K, 15 atm, and a 20cm path length for 10% H_2O in air, 10% CO_2 in air, 10% CO in air, and 1% CH_4 in air using the HITRAN database [2].

1.2 Absorption spectroscopy database for high pressures

These spectral simulations and the comparison with experiment require understanding the temperature, pressure, and gas composition influence on the lineshape function $\phi_{ij}(\nu)$. For the conditions in a gasifier, the lineshape is conveniently approximated by the convolution of a Doppler-broadened (Gaussian) term with a collision-broadened (Lorentzian) term; this convolution is called the Voigt lineshape. The Doppler term can be simply calculated from the temperature, but the collision term requires knowledge of the temperature-dependent collision

broadening spectroscopic data, which is collider dependent. The full-width at half-maximum of the collision broadening term is given by:

$$\Delta\nu_{c,i} = P\sum_{j} x_j 2\gamma_{ij}$$

where P is the pressure, sum is over the j species in the gas mixture, x_j the mole fraction of the j^{th} species (collision partner) and $2\gamma_{ij}$ the collision-broadening coefficient for j^{th} species collisions on the i^{th} species absorber. The collision-broadening coefficient is typically expanded in a power law in temperature:

$$\gamma_{ij}(T) = \gamma_{ij}(T_{ref}) \cdot \left(\frac{T_{ref}}{T}\right)^{n_j}$$

where T_{ref} is the reference temperature (typically 296 K) and n_j is the temperature-dependence index. HITRAN has broadening coefficients for collisions with air and self-collisions of the absorbing species; however, temperature-dependent broadening data for other species must be measured in the laboratory. For this work we considered collision broadening with the major species in syngas: CO, CO_2, H_2, H_2O, and N_2. Due to the relatively low mole fraction of CH_4 in syngas, collision broadening of the measured species (CO, CO_2 and H_2O) broadened by CH_4 was not investigated.

The spectroscopic parameters were measured by wavelength-scanned direct absorption as a function of pressure and temperature in a static cell of length 9.9 cm for CO, CO_2 and CH_4, and a different static cell of 76.2 cm length for H_2O, following the method of Arroyo et al.[3] The cell was first filled by a known quantity of pure gas and the lineshapes of the selected transitions were acquired, as illustrated for CO_2 in Fig. 3(a). The linewidth of the single mode diode laser (<0.0002 cm^{-1}) was neglected. The best Voigt fit of the measured lineshape was used to compute the integrated absorbance, which is proportional to the line strength and absorbing-species partial pressure, as discussed above. The linear slope of integrated absorbance versus pressure provided the line strength.

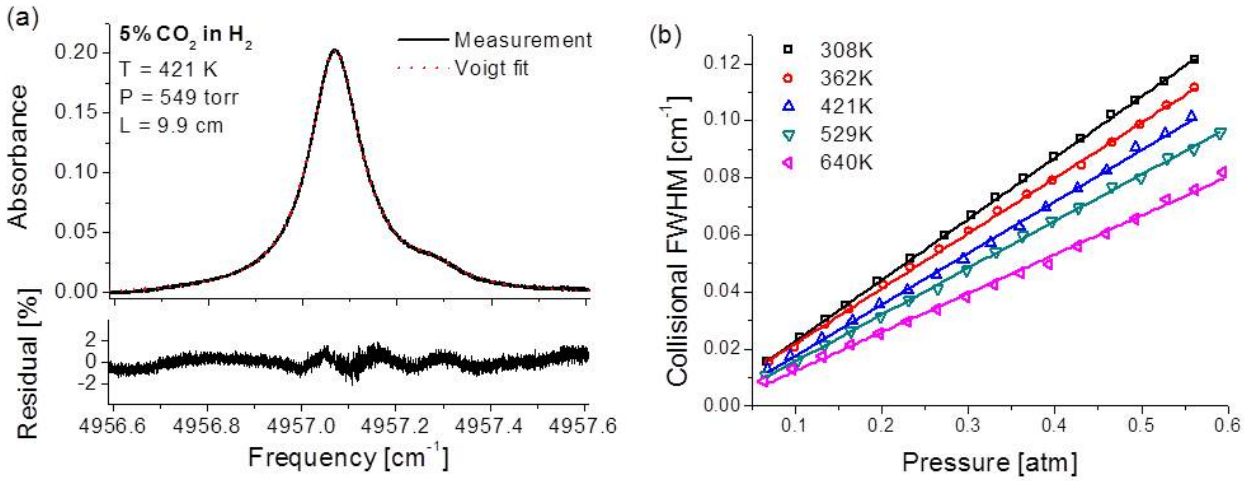

Figure 3(a) Sample direct absorbance spectra of CO_2 showing agreement with a Voigt fit; (b) Measured collisional FWHM for 5% CO_2 in H_2 at different pressures.

The collision-broadening coefficients were determined from the Lorentzian-halfwidth parameter from Voigt fits of the lineshape with the linestrength fixed. The self-broadening was first

determined over a range of pressures. Then, binary mixtures of the absorbing gas with a collision partner were studied and the absorption lineshape fit with only the width contribution of the collision partner allowed to vary. The slope of the fitted width versus pressure gave the broadening coefficient, the results of which are given in Table 1 [4]. A sample set of measurements for CO_2 broadening in H_2 is shown in Fig. 3(b). The uncertainty in the measured linestrengths and broadening (except water) was estimated to be within 1% and 2%, respectively, in the measured temperature range of 300 – 700 K. For water broadening, this uncertainty was larger due to the reduced range of binary mixture pressures and was estimated to be less than 5%. Armed with the needed collision broadening data, various modulation strategies could be examined.

1.3 Wavelength modulation spectroscopy for absorption measurements

There is a long (>30 year) history of WMS absorption measurements using injection-current-tuned diode lasers (TDL) [5-12]. Tunable diode lasers (TDLs) simultaneously vary laser intensity and output wavelength as the injection current is varied, and thus, when the injection current is used for the wavelength modulation, a simultaneous intensity modulation is produced. All of the n*f* components of the WMS signal are proportional to laser intensity, and at line center the WMS-1f term for injection-current tuned TDLs is dominated by the laser intensity contribution [13]. The simultaneous wavelength and intensity modulation of injection current tuned TDLs enables the 1*f*-normalization of the WMS-2*f* signal to avoid the need to scan on/off the transition for the zero absorption baseline used in the analysis of wavelength-scanned direct absorption and accounting for non-absorption losses in laser power due to scattering, window fouling or laser power drift. Quite early in the development of WMS using TDLs [14], the line center WMS-1*f* signal was used to normalize the WMS-2*f* signal, which during the measurements removed the need to scan the laser wavelength off the absorption transition to acquire a non-absorption baseline. For harsh environments this normalization can account for non-absorption variations of laser intensity, which has been exploited by several authors for sensors in a variety of harsh environments [e.g., 15-17].

WMS analysis requires understanding of the collision- and Doppler-broadened lineshape of the absorption transition as the WMS-2*f* signal has contributions from both lineshape and absorbance. Traditionally, WMS measurements have relied on an *in situ* calibration to avoid knowing the lineshape. Alternatively if the lineshape is known, this calibration measurement can be avoided (called "calibration free" by Rieker et al. [17]). In addition to temperature and pressure, the lineshape requires a reasonable estimate of the respective mole fractions of the major components of the test gas and a database of the pressure- and temperature-dependent coefficients for pressure broadening for each of the species in the gas mixture. This model-based approach to the lineshape is problematic for gasifier applications because the composition of the syngas is the primary target of the measurement. In our early work [18, 19], an iterative approach was able to make quantitative laser absorption measurements in syngas, for the first time. Unfortunately, this iterative approach is limited to post-processing data analysis and does not provide an opportunity for the real-time sensing needed for gasifier control applications. For wavelength-scanned direct absorption, the lineshape is determined from a fit to the measured absorption feature, and a combination of direct absorption to determine lineshape and WMS to determine absorption has been used in reactive flows [20]. But, again this scheme is limited to post-processing analysis.

Table 1. Measured spectroscopic parameters of the selected transitions

Carbon monoxide													
Line center [cm^{-1}]	Line strength (296K) [$cm^{-2}atm^{-1}$]	Lower state energy [cm^{-1}]	$2\gamma_{self}$ [8] [$cm^{-1}atm^{-1}$]	n_{self} [8]	$2\gamma_{N2}$ [8] [$cm^{-1}atm^{-1}$]	n_{N2} [8]	$2\gamma_{H2}$ [$cm^{-1}atm^{-1}$]	n_{H2}	$2\gamma_{CO2}$ [8] [$cm^{-1}atm^{-1}$]	n_{CO2} [8]	$2\gamma_{H2O}$ [8] [$cm^{-1}atm^{-1}$]	n_{H2O} [8]	
4297.70	0.0726	211.40	0.126	0.75	0.115	0.75	--	--	--	--	--	--	
4300.70	0.0649	253.67	0.124	0.71	0.114	0.70	0.147	0.55	0.144	0.69	0.252	0.96	
Carbon dioxide													
Line center [cm^{-1}]	Line strength (296K) [$cm^{-2}atm^{-1}$]	Lower state energy [cm^{-1}]	$2\gamma_{self}$ [$cm^{-1}atm^{-1}$]	n_{self}	$2\gamma_{N2}$ [$cm^{-1}atm^{-1}$]	n_{N2}	$2\gamma_{H2}$ [$cm^{-1}atm^{-1}$]	n_{H2}	$2\gamma_{CO}$ [$cm^{-1}atm^{-1}$]	n_{CO}	$2\gamma_{H2O}$ [$cm^{-1}atm^{-1}$]	n_{H2O}	
4957.08	0.02427	234.08	0.196	0.73	0.143	0.720	0.224	0.582	0.160	0.718	0.238	0.726	
4958.97	0.02648	197.41	0.200	0.68	0.145	0.700	--	--	--	--	--	--	
Methane													
Line center [cm^{-1}]	Line strength (296K) [$cm^{-2}atm^{-1}$]	Lower state energy [cm^{-1}]	$2\gamma_{self}$ [$cm^{-1}atm^{-1}$]	n_{self}	$2\gamma_{N2}$ [$cm^{-1}atm^{-1}$]	n_{N2}	$2\gamma_{H2}$ [$cm^{-1}atm^{-1}$]	n_{H2}	$2\gamma_{CO}$ [$cm^{-1}atm^{-1}$]	n_{CO}	$2\gamma_{CO2}$ [$cm^{-1}atm^{-1}$]	n_{CO2}	$2\gamma_{H2O}$ [$cm^{-1}atm^{-1}$]	n_{H2O}
4367.00	0.118	104.77	0.144	0.78	0.136	0.74	0.132	0.38	0.139	0.58	0.166	0.64	0.150	0.97
Water														
Line center [cm^{-1}]	Line strength (296K) [$cm^{-2}atm^{-1}$]	Lower state energy [cm^{-1}]	$2\gamma_{self}$ [$cm^{-1}atm^{-1}$]	n_{self}	$2\gamma_{CO}$ [$cm^{-1}atm^{-1}$]	n_{CO}	$2\gamma_{CO2}$ [$cm^{-1}atm^{-1}$]	n_{CO2}	$2\gamma_{N2}$ [$cm^{-1}atm^{-1}$]	n_{N2}	$2\gamma_{H2}$ [$cm^{-1}atm^{-1}$]	n_{H2}		
7393.79	0.0178	744.06	0.478	0.73	0.128	0.800	0.150	0.959	0.093	0.547	0.082	0.462		
7393.85	0.0512	744.16	0.530	0.65	0.119	0.620	0.139	0.957	0.088	0.575	0.082	0.463		

For practical long term measurements, a modulation strategy that is immune to long term drift of the laser wavelength is needed. But unfortunately, the simultaneous wavelength and intensity modulation complicates the analysis of the complete WMS lineshape, and until recently quantitative interpretation of the full lineshape of wavelength-scanned 1*f*-normalized WMS-2*f* was quite difficult. However, Stanford has recently developed a new paradigm for the acquisition and analysis of wavelength-scanned WMS [21, 22] with partial support of this grant. This development is captured in the patent application noted in the publications section of this report. In this new method, the wavelength-scanned 1*f*-normalized WMS-2*f* signals are fit with only the lineshape defined by the collision-broadened FWHM and the peak absorbance as free parameters. The details of the analysis and fitting of this new wavelength-scanned WMS method are briefly described here and the details can be found in the published literature [21, 22].

Here we only review the key steps used to simulate the WMS-n*f* absorption signals to guide the discussion.

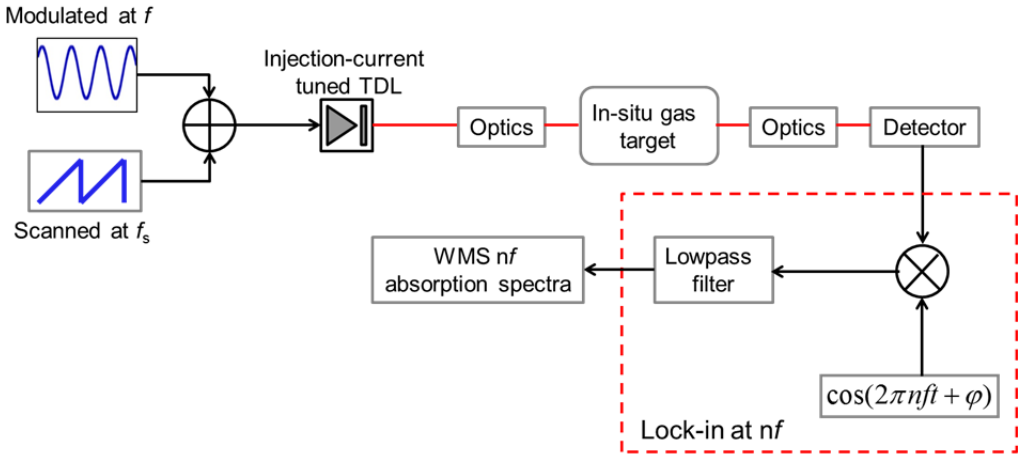

Figure 4. Schematic of the experimental setup of a typical WMS measurement and approaches to obtain the WMS-n*f* absorption spectra.

For typical wavelength-scanned measurements (see Fig. 4), the laser wavelength is modulated rapidly by varying its injection current at frequency f superimposed upon a slow scan of the mean injection-current of the modulated laser at frequency f_s . The laser wavelength and intensity are simultaneously modulated and ramped by this variation of injection current.

The intensity variation as a function of time $I_{bg}(t)$ is measured by the photodiode detector during sensor setup with no absorber present in the laser line-of-sight (LOS). The simultaneous wavelength modulation and scan for a single scan can be described as:

$$\nu(t) = \bar{\nu} + a\cos(2\pi ft + \varphi_\nu) + F(t),$$

where $\bar{\nu}$ is the laser frequency (or wavelength) without injection-current tuning, a [cm^{-1}] the modulation depth, φ_ν the phase of the frequency modulation, and $F(t)$ the function describing the wide near-linear wavelength scan, normally a polynomial of three to four orders. The absorption of the time-varying intensity is described by Beer-Lambert's law, and the simulated transmitted laser intensity ${}^{S}I_t(t)$ can be expressed as:

$$^{S}I_t(t) = I_{bg}(t) \cdot \exp[-\alpha(\nu(t))],$$

where $\alpha(\nu(t))$ is written:

$$\alpha(\nu(t)) = \exp\left(-\sum_j S_j \cdot \phi_j(\nu(t)) \cdot P \cdot x_i \cdot L \right).$$

Here S_j and ϕ_j are the linestrength and lineshape function of transition j, P the total pressure of the gas, x_i the mole fraction of absorber i and L the pathlength. The product of $S_j \cdot P \cdot x_i \cdot L$ is defined as the absorbance area or the integrated absorbance. For known pressure, temperature, and pathlength, the absorber mole fraction can be determined from the absorbance area if the linestrength is known.

The Voigt lineshape [23] of a relatively isolated absorption transition is used here and is given by the convolution of a Doppler broadening component (Gaussian) and a collisional-broadened component (Lorentzian). For the high-pressure applications studied here, the Voigt lineshape function can be approximated by a Lorentzian lineshape:

$$\phi = \frac{1}{2\pi} \frac{\Delta\nu_c}{(\nu - \bar{\nu})^2 + \left(\frac{\Delta\nu_c}{2}\right)^2}$$

where $\Delta\nu_c$ is the collisional width of the transition. In the limit of binary collisions the width is proportional to pressure at constant temperature, and for a multi-component gas mixture, the total collisional width can be obtained by summing the contributions from all components:

$$\Delta\nu_c = 2 \cdot P \cdot \sum_j x_j \cdot \gamma_j(T)$$

where x_j is the mole faction of species j, and γ_j is the broadening coefficient due to collisions by the j^{th} species. The relationship between γ_j and T can be described as:

$$\gamma_j(T) = \gamma_j^{296K} \cdot \left(\frac{296}{T}\right)^{n_j}$$

where n_j is the temperature exponent of the collisional broadening coefficient.

A digital lock-in is then used to shift the n*f* harmonic components from n*f* frequency to zero frequency, by multiplying the simulated ($^{S}I_t(t)$) and measured ($^{M}I_t(t)$) transmitted laser intensities by $\cos(n \cdot 2\pi ft)$ for the X-component (real) and $\sin(n \cdot 2\pi ft)$ for the Y-component (imaginary). A numerical lowpass filter with a bandwidth less than *f*/2 is then used to extract these components:

$$X_{nf} : I_t(t) \cdot \cos(n \cdot 2\pi ft) \rightarrow \text{lowpass filter.}$$

$$Y_{nf} : I_t(t) \cdot \sin(n \cdot 2\pi ft) \rightarrow \text{ lowpass filter.}$$

The absolute magnitude of the WMS-n*f* signal is then given as:

$$S_{nf} = \sqrt{X_{nf}^2 + Y_{nf}^2} \ .$$

To account for time varying non-absorption transmission losses, the 1*f* signal can be used to normalize the n*f* signal:

$$S_{nf_{normalized}} = S_{nf} \ / \ S_{1f}$$

Analogous to wavelength-scanned DA, the integrated absorbance area (or the absorber mole fraction if the linestrength, pressure, temperature and pathlength are known) and the collisional width of the transition can be varied to achieve the best fit between the simulation and the measurement for each normalized WMS-n*f* absorption spectrum.

1.4 Laboratory experiment to test WMS analysis scheme

A transition near 7393.84cm^{-1} (lower state energy, E" ~ 744cm^{-1}) was selected to probe H_2O mole fraction in the gasifier output (see fig. 5). The absorption feature is in fact two closely spaced transitions with the same E" positioned at 7393.79cm^{-1} and 7393.84cm^{-1}. The laboratory measured spectroscopic data[4] and HITRAN database[2] suggest this line pair can be considered as a single transition with one set of line broadening parameters at high pressure. The spectroscopic data for this transition are listed in Table 2. This transition pair was selected for four reasons: (1) the absorption is strong at the measurement temperature (near 600K), providing good signal-to-noise ratio in gasifier environment; (2) the transition is well isolated from neighbors at elevated pressures; (3) the 2*f*/1*f* absorption signal is not sensitive to temperature changes in the region near 600K; (4) and the collisional width is small, providing narrow lineshape to enhance WMS signals. Note that here and throughout the paper the SNR is defined as the ratio of the 1*f*-normalized WMS-2*f* peak signal to the standard deviation of the residual WMS model fit.

Table 2. Laboratory measured spectroscopic parameters (linestrength, collisional-broadening coefficients and their temperature dependence exponents (in the parenthesis)) at 296K for the target transition using the procedure from [3].

Linecenter [cm^{-1}]	Linestrength [cm^{-2}atm^{-1}]	Lower state energy [cm^{-1}]	$2\gamma_{H2O\text{-}H2O}$ [cm^{-1}atm^{-1}] ($n_{H2O\text{-}H2O}$)	$2\gamma_{H2O\text{-}CO2}$ [cm^{-1}atm^{-1}] ($n_{H2O\text{-}CO2}$)	$2\gamma_{H2O\text{-}CO}$ [cm^{-1}atm^{-1}] ($n_{H2O\text{-}CO}$)	$2\gamma_{H2O\text{-}N2}$ [cm^{-1}atm^{-1}] ($n_{H2O\text{-}N2}$)	$2\gamma_{H2O\text{-}H2}$ [cm^{-1}atm^{-1}] ($n_{H2O\text{-}H2}$)
7393.84	0.0690	744	0.530 (0.650)	0.139 (0.957)	0.119 (0.620)	0.088 (0.575)	0.082 (0.463)

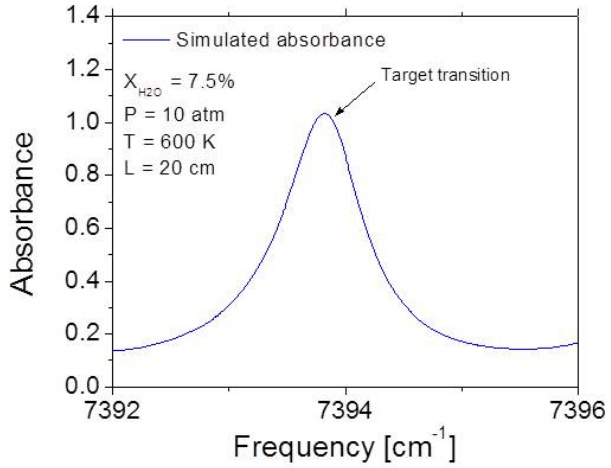

Figure 5. Simulated absorption spectrum for H_2O molecule at typical gasifier conditions.

To validate the H_2O sensor in the laboratory, absorption near 7394cm^{-1} was measured for a known H_2O mole fraction as a function of pressures in a 100.5cm-long cell at room temperature (Fig. 6). The cell was first evacuated to measure a background signal, then filled with an H_2O/air mixture at constant pressure. The mixture was premixed and stored overnight to ensure homogeneity. A DFB laser (NEL) near 1352 nm with single-mode fiber output was used to probe the H_2O transition near 7394.8cm^{-1}. The laser injection current was modulated with a sine function at 10 kHz, superposed on a sawtooth function at 25 Hz. Computer-driven outputs (National Instruments PCI-6115) controlled the diode laser injection current (ILX Lightware LD-3900). After collimation, the laser beam travelled through the cell and was focused onto a NIR photo-diode detector (Thorlabs PDA-10CS). The voltage signal on the gain-adjustable detector was then sampled (National Instrument, PCI-6115, 12 bit, ac-coupled) and numerically post-processed by using a lock-in program and a digital FIR low-pass filter (bandwidth of 2 kHz). The line-of-sight (LOS) pathlength external to the cell was purged by pure N_2 gas to minimize absorption from ambient atmospheric moisture.

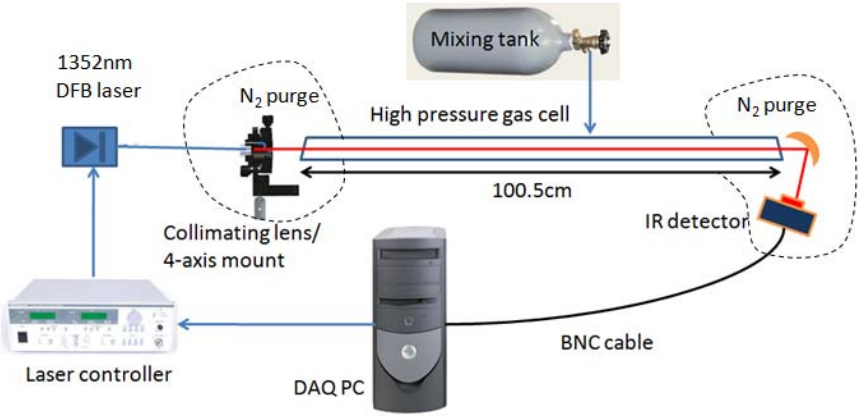

Figure 6. Laboratory measurement setup for validation of the wavelength-scanned WMS strategy for high-pressure gas sensing.

Figure 7 shows the measured 1*f*-normalized WMS-2*f* spectrum at three different modulation depths as well as the best-fit results at known conditions of P = 10atm, T = 296K. The calibrated H_2O moisture mole fraction in the mixture is 0.096% and the expected FWHM collisional width is 0.81cm^{-1} ($2\gamma_{H_2O-Air}$ = 0.081cm^{-1}/atm, determined by DA measurements at sub-atmospheric pressures). The WMS analysis procedure [21, 22] includes the laser intensity modulation (to all orders) and we speculate this difference results from the imprecision of the spectral model, for two reasons: (1) The lineshape at high pressures can be non-Voigt due to line mixing and other phenomena. (2) The signal can include contribution from collision broadening of neighboring transitions, which can be more significant in the wings of the lineshape. Nevertheless, the overall comparison reveals better than 2% H_2O mole fraction agreement, demonstrating the feasibility of using the 1*f*-normalized wavelength-scanned WMS-2*f* strategy for simultaneous determination of absorber mole fraction and collisional width of the transition at high pressures.

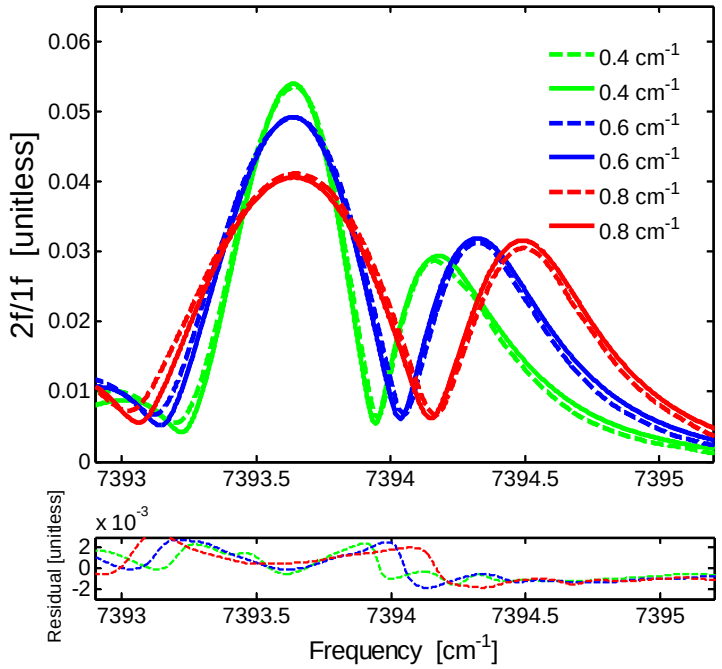

Figure 7. Measured single-sweep WMS-2*f*/1*f* lineshape using different modulation depths and the best fit results (best fit parameters: for a = 0.4cm^{-1}, x_{H2O} = 0.0953% , $\Delta\nu_c$=0.823 cm^{-1}, for a = 0.6cm^{-1}, x_{H2O} = .0947% , $\Delta\nu_c$ =0.820 cm^{-1}, for a = 0.8cm^{-1}, x_{H2O} = 0.0961% , $\Delta\nu_c$ =0.802 cm^{-1}) . Lower panel shows the residuals of the fit are <2% of the signal.

Figure 8 presents the collisional widths, integrated absorbance and the resulting H_2O mole fractions that best fit the measured WMS absorption spectra at pressures ranging from 3.2 atm to 15.8 atm, measured with a modulation depth of 0.8 cm^{-1}. The small deviation (< 1.3%) between the measurements and the expected values indicates that: (1) the fitting strategy for wavelength-scanned WMS simultaneously yields the transition integrated absorbance and collisional width, even at high pressures up to 15.8 atm; (2) the non-ideal Lorentzian behavior, such as line-mixing and the finite-collision breakdown do not have significant influence on determining the gas parameters (i.e. mole fraction) for this target transition and this range of conditions.

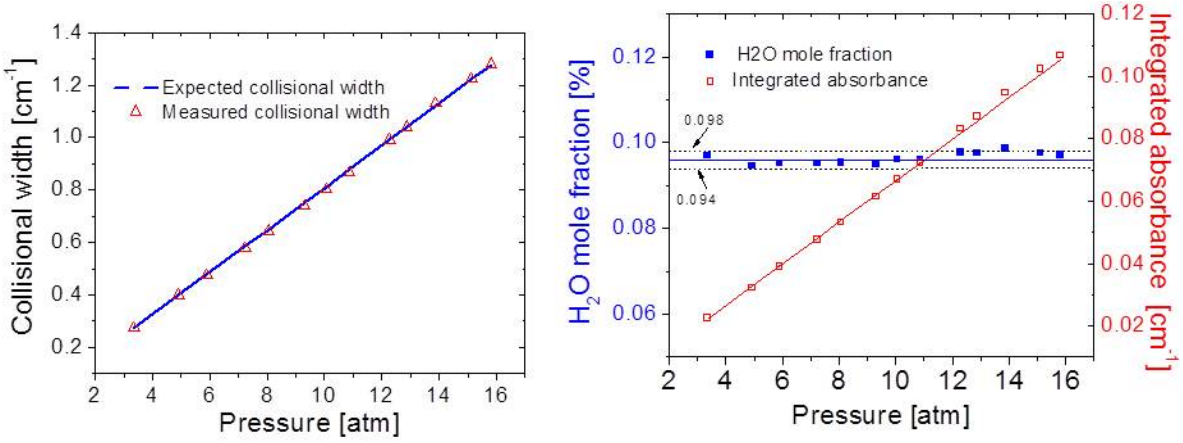

Figure 8. Best-fit results for the transition collisional width (left panel) and integrated absorbance and mole fraction (right panel) at different pressures. (T = 296K, L = 100.5cm).

2. Laboratory validation of sensor performance

Using the measured spectroscopy data to augment the HITRAN database, WMS measurements of absorption were optimized for the measurement of CO, CO_2, CH_4 and H_2O using four lasers wavelength tuned across transitions near 4301, 4957, and 4367 (Nanoplus), and 7394 (NEL) cm^{-1} (2325, 2017, 2290, and 1352 nm, respectively). The calculated WMS lineshape was then compared with measurements to validate the measurement method. First, the target gas was diluted in nitrogen at known mole fractions, and measurements were made in known mixtures of target gas and synthetic syngas. With the assumption that the remainder of the gas was H_2, the heating value and the Wobbe index of the syngas was calculated from these laboratory measurements and compared with the known value of the gas mixture. The details of this work were published [4] in the peer-reviewed literature and the results summarized here.

The magnitude of the 1*f*-normalized WMS-2*f* signal varies strongly with the modulation depth, and the optimum modulation depth was selected for use at elevated pressures. Generally, at higher pressure, the WMS signals become smaller due to the reduction in spectral curvature. Therefore, the modulation depth was optimized to enhance the higher-pressure signals. As an example, Fig. 9 shows the case for the 2.0 μm laser for detection of CO_2 in a sample syngas-like mixture containing 30% CO, 30% CO_2, 15% H_2, 15% N_2 and 10% H_2O. The modulation depth selected optimized the signal strength at 20 atm while retaining as much signal strength as possible at lower pressure. For CO, the optimum modulation depth could not be reached as a result of the limitation of the laser tuning characteristics. The selected modulation depths for these sensors are listed in Table 3.

Table 3. Selected modulation depth for the sensors

Species	Selected modulation depth [cm^{-1}]
CO	0.58
CO_2	0.76
CH_4	1.02
H_2O	1.08

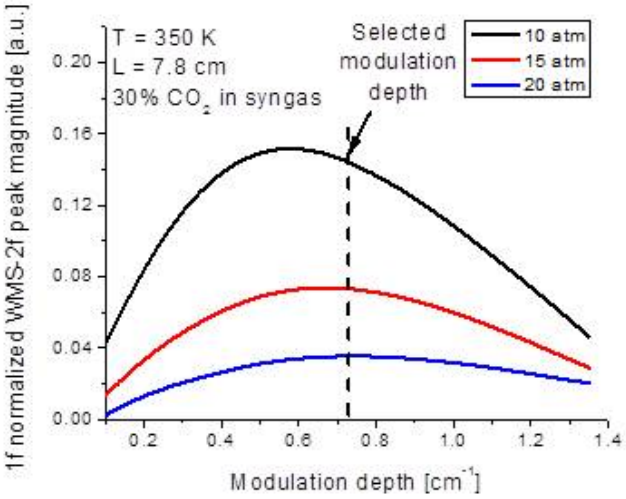

Figure 9. Variation of 1f normalized WMS-2*f* magnitude at the selected peak wavelength near 2017 nm for CO_2 detection with modulation depth at a 10 kHz modulation frequency at gas pressures between 10 and 20 atm.

2.1 Sample WMS measurements of species in N_2 at elevated pressure

The first validation experiments were conducted for the target species dilute in nitrogen. The measured the 1*f*-normalized WMS-2*f* spectral lineshape for the target transition was compared with spectra simulated using the HITRAN/HITEMP database augmented by our measured pressure-broadening data. As observed from Fig. 10, the WMS spectra for CH_4 and CO show very good agreement with the simulations (data for H_2O and CO_2 showed similar good agreement). These measurements confirm that other high-pressure phenomena that were not considered, such as line mixing and other non-Lorentzian effects, can be ignored in this pressure range for the target transitions.

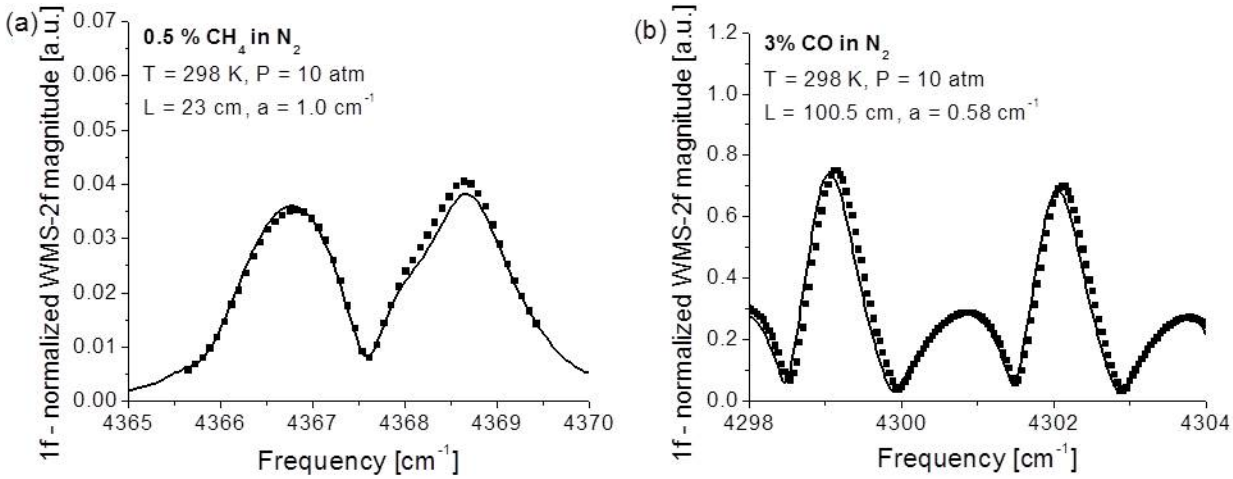

Figure 10. **Sample WMS lineshapes simulated and measured for (a) CH_4 and (b) CO in N_2 at 10 atm.**

2.2 WMS measurements in synthetic syngas versus pressure

After experimental verification of the lineshape of species dilute in nitrogen (up to 20 atm), the sensor was tested in mixtures of synthetic syngas with varying concentrations of target species as a function of pressure. A standard synthetic synagas mixture containing 25% CO, 25% H_2, 0.6% CH_4 and balance (49.4%) CO_2 was used to prepare the gas samples. Varying amounts of pure gas for one of the target species was then mixed with this base synthetic syngas. WMS lineshape measurements were made for different pressures in a room temperature, high-pressure cell, with a path length of 23 cm.

2.2.1 Carbon monoxide

The CO laser absorption has the strongest absorption strength and the target transition is well-isolated even at 20 atm. This leads to a very large WMS signal level at all the pressures investigated: 5, 10, 15 and 20 atm (Fig. 11 shows examples at 5 and 20 atm). The good agreement between the simulations and the measurements, especially for the peak near 4300.7 cm^{-1}, is evident from these figures.

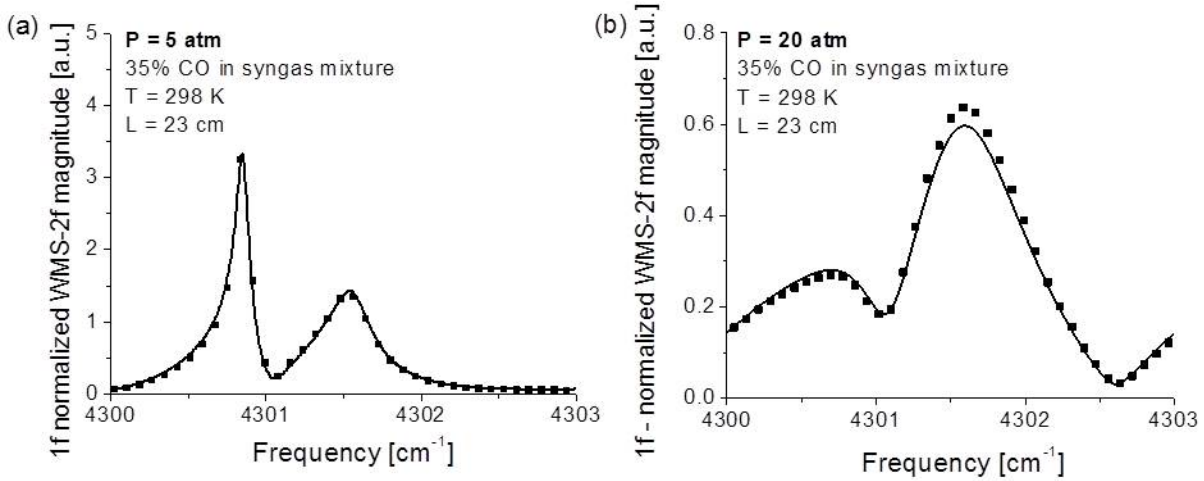

Figure 11. Measured and simulated WMS lineshapes for CO dilute in synthetic syngas at 5 and 20 atm.

8.2 Carbon dioxide

The CO_2 absorption spectrum is severely blended at pressures greater than 5 atm, which reduces WMS signal strength. Measured and simulated 1*f*-normalized WMS-2*f* lineshapes for CO_2 in a typical syngas mixture at 25°C and at pressures of 5 and 20 atm are shown in Fig. 12 (a) and (b), (c) and (d). The peak of the WMS lineshape near 4957 cm^{-1} agrees with the simulations over the full range of pressure.

8.3 Methane

Similar measurements for CH_4 at a temperature of 25°C and pressures of 5 and 20 atm are shown in Fig. 13. The methane absorption feature is not a single transition but consists of multiple lines that are blended by pressure broadening. In spite of these complications, the simulation and measurement are in quite good agreement and these results serve to verify the accuracy of the spectral database.

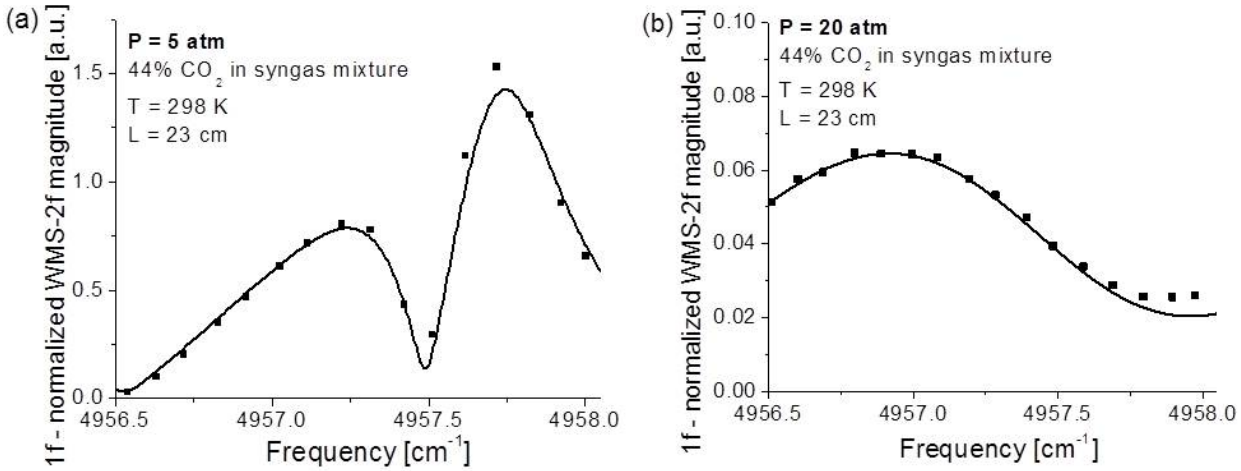

Figure 12. Measured and simulated WMS lineshapes for CO_2 dilute in synthetic syngas at 5 and 20 atm.

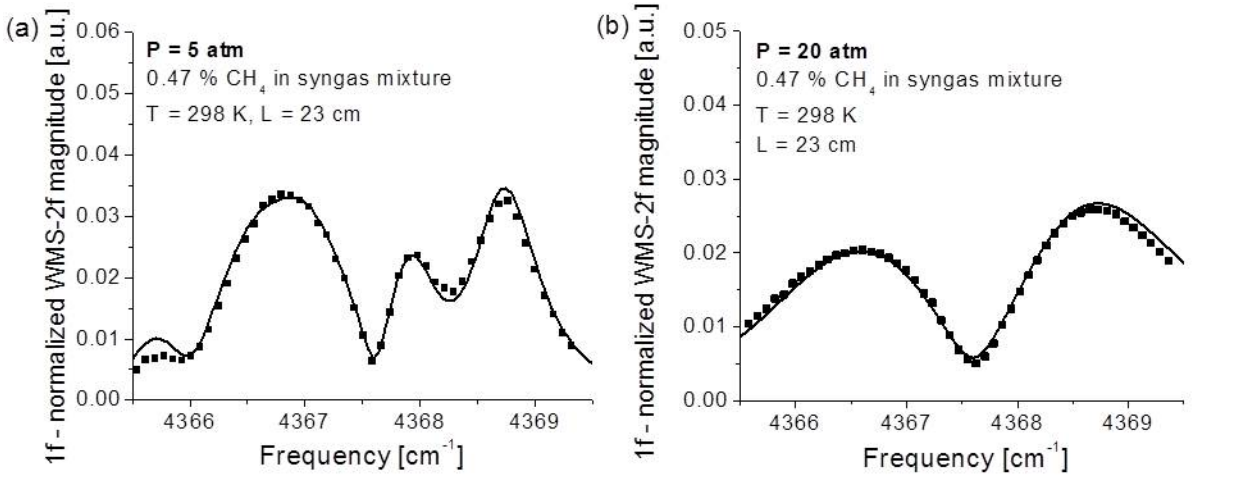

Figure 13. Measured and simulated WMS lineshapes for CH_4 dilute in synthetic syngas at 5 and 20 atm.

2.3 Summary of the laboratory validation experiments

The comparison of laser absorption measurements of the target species in synthetic syngas are compared with known values for all the mixtures and pressures in Fig. 14. Each measurement was repeated three times at the same mole fraction of CH_4 and two times for CO with different mixture compositions. The known mixtures were prepared by volumetric addition of varying amounts of one of the components with the base mixture of 25% CO, 25% H_2, 0.6% CH_4 and balance (49.4%) CO_2. The mixture compositions used for the validation experiments are listed in Table 4. Measured data points agree with the known values within 4%, 4% and 8% (1%, 2% and 0.05% of total) of the measurements of the mole fraction of CO, CO_2 and CH_4, respectively. These measurements were done as a function of pressure and the general trend reflects a small increase of the difference between measured and known values with increasing pressure. The WMS signal becomes increasingly sensitive to the broadening parameters at higher pressures and these differences can be attributed to the uncertainties in the broadening coefficients. Some part of the high-pressure differences might be also attributed to non-Lorentzian behavior of gases at higher pressures such as line-mixing and finite duration of collisions.

Table 4. Percentage compositions of components in the mixtures used for the sensor validation experiments

CO	CO_2	CH_4	H_2
25.0	49.6	0.6	24.8
35.0	44.0	0.5	20.5
20.1	41.0	0.5	38.4
20.1	60.0	0.5	19.4

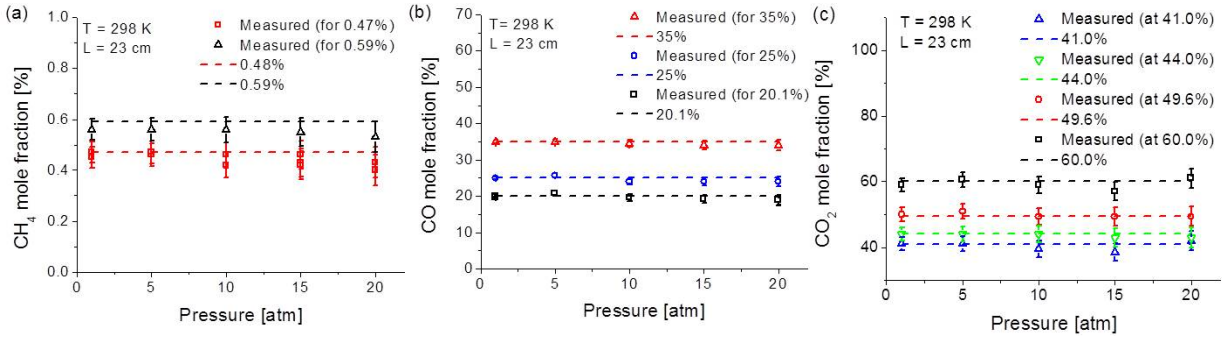

Figure 14. Comparison of the known and the measured values of (a) CH_4, (b) CO and (c) CO_2 mole fractions in syngas mixtures.

2.4 Calculation of LHV and Wobbe Index of syngas mixture

The lower heating value (LHV) of a fuel is used widely to compare the potential heat release from burning for different fuels. This is the chemical heat release for the transition of fuel to complete combustion at 25°C and 1 atm with saturated water vapor in the products. When characterizing the LHV output from a gasifier, the mass basis is often chosen to be the mass of the reacted carbon present in syngas, to include the efficiency of the gasification process of solid coal.

The syngas-like mixtures are primarily composed of CO, CO_2, CH_4, H_2O and H_2 along with many trace species such as H_2S, NH_3, etc. The laser absorption sensors described here can measure all the components except H_2, which is assumed to be the balance for an oxygen-blown process (although here the trace species are ignored, these species could also be measured with laser absorption). This assumption provides a path to infer the lower heating value (in MJ/Kg C) of the syngas as:

$$LHV = \frac{\left[\Delta H^0_{f,H_2O(g)}\right]\cdot x_{H_2} + \left[\Delta H^0_{f,CO_2} - \Delta H^0_{f,CO}\right]\cdot x_{CO} + \left[2\Delta H^0_{f,H_2O} + \Delta H^0_{f,CO_2} - \Delta H^0_{f,CH_4}\right]\cdot x_{CH_4}}{M_C \cdot \left[x_{CO} + x_{CO_2} + x_{CH_4}\right]}$$

where x_i is the mole fraction, $\Delta H^0_{f,i}$ is the standard heat of formation and M_i is the molar mass of the species i. The subscript (g) indicates the gaseous phase of water. Here, the parameters were calculated from the NIST-JANAF [24] tables and the bimolecular species H_2 and O_2 are reference species and hence have a zero heat of formation (ΔH^0_f) at 25°C. This method of obtaining the LHV is valid only for oxygen-blown gasifiers which have low concentrations of

fuel nitrogen in the syngas stream. For air-blown systems or systems with significant nitrogen purge, N_2 must also be accounted in the syngas mixture.

Another parameter of importance when dealing with modern gaseous fuels is the Wobbe Index (WI), which is a measure of interchangeability of fuels. It is expressed as:

$$WI = \frac{HHV}{\sqrt{G_s}} = \frac{\left[\Delta H^0_{f,H_2O(l)}\right]\cdot x_{H_2} + \left[\Delta H^0_{f,CO_2} - \Delta H^0_{f,CO}\right]\cdot x_{CO} + \left[2\Delta H^0_{f,H_2O} + \Delta H^0_{f,CO_2} - \Delta H^0_{f,CH_4}\right]\cdot x_{CH_4}}{\sqrt{G_s}}$$

where G_s is the specific gravity of the gaseous fuel with respect to dry air at 25°C and 1 bar. The subscript (l) indicates the liquid phase of water.

The lower heating value was calculated per kilogram carbon basis for each of the syngas mixtures, and compared to the known value in Fig. 15(a). A maximum scatter of less than 6% (rms error < 0.4%) was observed for all these measurements. Similarly, comparison between the measured and the known values of the Wobbe Index are in good agreement as apparent from Fig. 15(b). The maximum scatter observed in this case was below 8% (rms error < 0.4%). The effective uncertainty in these inferred values from the constituents was due to the cumulative uncertainty in each of the measured components.

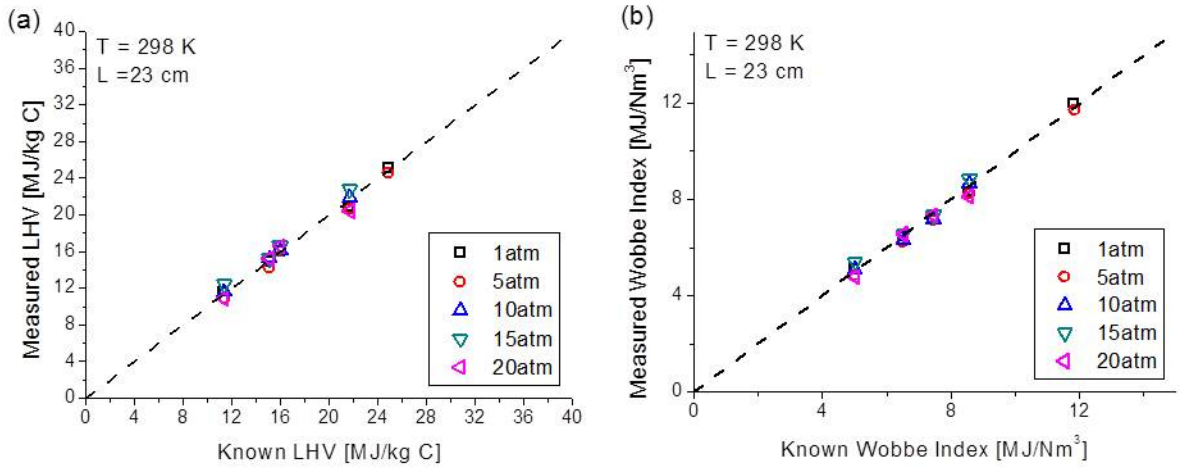

Figure 15. Comparison of known and measured (a) LHV in MJ/kg C; (b) Wobbe index in MJ/Nm^3.

2.5 Summary of sensor validation

Multi-laser-absorption sensors were designed, constructed and tested to monitor the mole fraction of CO, CO_2, CH_4 and H_2O in synthesis gas mixtures at pressures up to 20 atm and temperatures of 300 - 400 K. The sensor design was based on 1*f*-normalized WMS-2*f* detection of infrared laser absorption. The line selection was optimized for performance at high pressures and to suppress interference from typical syngas composition. A database of collision-broadening coefficients was acquired for collisions with the set of species (CO, CO_2, H_2, H_2O, N_2 and CH_4) expected in syngas. The performance of these sensors was evaluated at room temperature up to a pressure of 20 atm. The spectral simulations for the 1*f*-normalized WMS-2*f* signals showed agreement with the measurements in both binary mixtures with N_2 and in multi-

species synthetic syngas. The lower-heating value and the Wobbe index were calculated from the sensor data and compared with the known values. The inferred values were within 6% for the LHV and 8% for the Wobbe index over the entire pressure range. The sensor has the potential to become a reliable and fast real-time monitor for gasifier product syngas composition, with a promising future for new strategies of gasification control. The use of this four species sensor in a pilot-scale gasifier at the University of Utah and an engineering-scale gasifier at NCCC is discussed below.

3. Field measurements in a pilot-scale research coal gasifier

A series of four field measurement campaigns (August 2010, December 2010, August 2011, and June 2012) were conducted to evaluate the feasibility of *in situ* laser absorption sensing in the syngas output from a pilot-scale entrained-flow coal gasifier at the Institute for Clean and Secure Energy at the University of Utah (Utah participation involved a subcontract with Professor Kevin Whitty at the U. of Utah). Between each measurement campaign the prototype laser sensor and the optical access windows in the gasifier were redesigned and improved to address the lessons learned in the previous campaign. The development of reliable, leak-free, safe optical windows for *in situ* laser absorption in the syngas flow was crucial to the eventual success of the sensor strategy. The June 2012 campaign included successful time-resolved measurements of CO, CO_2, CH_4 and H_2O for gasifier operation periods exceeding ten hours, and this work is described in detail in a peer reviewed publication [25] and summarized below.

3.1 The gasifier at the University of Utah

The Utah, pilot-scale (1 Ton coal per day) oxygen-blown, entrained-flow, down-fired, slagging coal gasifier can be broken down into four sections as shown in Fig. 16:

Section 1. Reactor core: A slurry of micronized coal and water, as well as pure oxygen, are fed through the nozzle at the top of this section. The water in the slurry instantly vaporizes upon introduction to the hot reactor core (1300K-1700K). The coal undergoes devolatilization, pyrolysis and finally gasification. Section 1 hosts most of the partial oxidation reactions. This region is characterized by extremely high particulate density and slag formation.

Section 2. Pre-quench section: After the reacted gas mixture exits the reactor core, it is cooled down by a spray of liquid water directed into the flow. This reduces the temperature to a value in the range 600K-1000K. The gas composition "freezes" corresponding to equilibrium at this temperature.

Section 3. Post-quench section: The syngas, after being quenched to a colder temperature by the water sprays in the previous section, bubbles out through a column of liquid water and is then conveyed through a pipe. At this location, the temperature of the gas is in the range 340K-400K. In [19] agreement of 2-line TDLAS based temperature measurements with the thermocouple readings was demonstrated. For the measurements here, the gas temperature was determined by thermocouples placed in the flow stream.

Section 4. Post-filtration section: The syngas is passed through a filtration unit to remove the particulates (unreacted coal, soot or ash) from the flow. The temperature does not drop

significantly between section 3 and this point. The difference is around 20 K. The overall temperature range is 320K-380K.

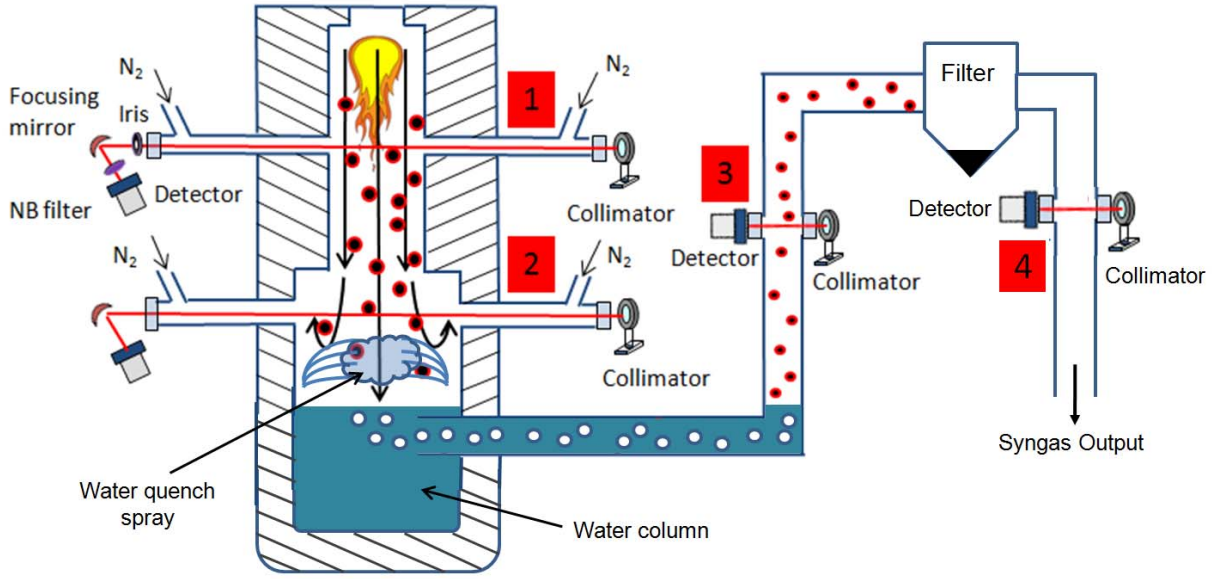

Figure 16. Schematic of the entrained flow gasifier at the Institute for Clean and Secure Energy at the University of Utah. The sections 1-4 are identified in the diagram.

TDLAS measurements of H_2O and temperature were performed at sections 1 and 2 and reported in [19] using amplified diode lasers. The lower power and less-robust fiber-coupled lasers available in the 2 - 2.3 µm region needed for CO, CO_2 and CH_4, limited the multi-species measurements to sections 3 and 4. Note, however, that the multi-species monitoring of syngas energy content is most useful at the gasifier exit (section 4).

3.2 Optical engineering for installation of laser absorption sensor

The lasers, along with the laser current/temperature controllers and the data acquisition (DAQ) system, were located about 1 m away from the optical access windows in the syngas output from the gasifier, and was remotely controlled from a room ~30m away from the high-pressure gasifier. It was necessary to locate the lasers near the rig because the optical fiber in the 2-2.3µm region available in 2012 had huge bend losses and the fiber lengths were limited to less than 2m for this version of the prototype sensor.

In situ laser absorption measurements require windows on the syngas flow line that can withstand the elevated pressure, temperature and corrosive gas contact. Here we used 2.5 cm thick sapphire windows sealed by Teflon gaskets. Sapphire was chosen due to its superior infrared transmission, physical strength and resistance to chemical attack. The thickness of the windows ensured safe operation for pressures up to 100 atm. To avoid water condensation on the windows, the window housing was electrically heated to maintain the window temperature (about 150°C) well above the water vapor saturation temperature.

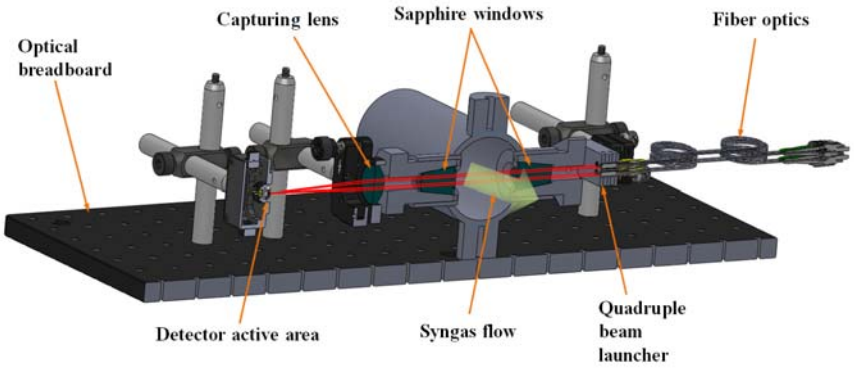

Figure 17. Free-space multiplexing of four laser beams onto a single detector.

As illustrated above in Fig. 2, the absorption linestrengths for the selected CO and H_2O absorption transitions were significantly stronger than those for CO_2 and CH_4. The absorbance is the product of linestrength, mole fraction and pathlength, and the expected mole fractions for CO and H_2O are larger than for CO_2 and CH_4. Thus, an increase in pathlength for the CO_2 and CH_4 detection, would allow all four species to be detected with similar signal to noise ratio. Therefore, the prototype sensor used at section four illustrated in Fig. 17 exploited a longer optical path (17.9 cm) for CO_2 and CH_4 than for CO and H_2O (8cm). Note this arrangement also simplified the laser multiplexing as only two lasers needed to be combined on each optical path. The typical multiplexing solution would combine beams on 50% beam splitters. Unfortunately that solution would reduce the power for each laser beam by a factor of 2. Thus, a parallel beam solution was designed as illustrated in Fig. 17. Two closely spaced beams were directed across the syngas flow, collected by an aspheric CaF_2 lens, and focused onto an extended-InGaAs detector (Thorlabs).

3.3 Laser absorption measurements in the Utah gasifier

The sensor performance was evaluated during a field measurement campaign at the Institute for Clean and Secure Energy (ICSE), University of Utah, Salt Lake City, Utah during the first week of May 2012. These results can be divided into two segments: 1) Wavelength-scanned measurements to confirm interference-free species measurements and 2) Simultaneous time-resolved multi-species concentration measurements to determine energy content of the gas.

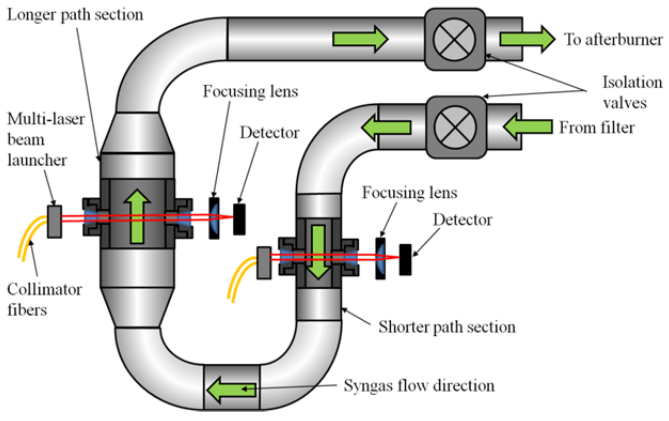

Figure 17. Schematic of the optical access assembly in Section 4; note the shorter (CO and H_2O) and the longer (CH_4 and CO_2) optical path locations.

Investigation of interference: The coal gasifier presents an extremely harsh environment that has the potential to produce unknown interfering species at the selected laser wavelengths. To investigate the possibility of interference, a scan over a wide wavelength range was made for each laser at each selected transition. Comparison of measurement and simulation of the shape of the WMS lineshape is used to reveal any significant interference absorption. For example, earlier measurements identified interference by NH_3 in the gas mixture, which led to an alternate selection of a CH_4 transition (used here) devoid of this NH_3 interference. Such measurements were performed for CO, CO_2, CH_4 and H_2O and compared to the expected WMS lineshape as shown in Fig. 18. Agreement of the 1*f*-normalized WMS-*2f* lineshapes with the simulated spectra confirms the identity of the absorbing species, yields a high signal to noise ratio of the obtained signals and verifies the absence of significant interference for any of the selected transitions.

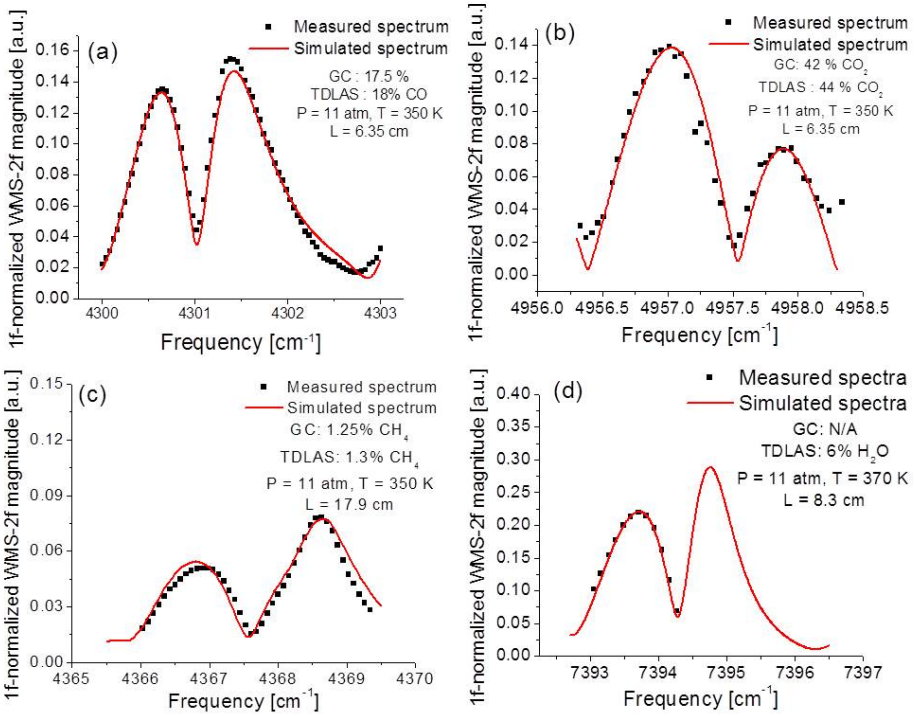

Figure 18. Sample WMS lineshape spectra for (a) CO, (b) CO_2, (c) CH_4 and (d) H_2O measured in the syngas products of coal gasification at 11 atm.

Simultaneous time-resolved multi-species concentration measurements: Time-resolved concentrations of the four target species were monitored during a series of gasifier runs with typical time resolution of 0.33 Hz. The laser absorption measured mole fractions at section 3 are compared with data from a GC (Varian CP-4900, repeatability < 0.5% measured value). Figure 19 displays the simultaneous laser absorption measurements of CH_4, CO, CO_2 and H_2O at section 3 and GC data for CH_4, CO and CO_2. To compare with the GC measurements (which can only analyze dry gases), the laser absorption mole fraction measurements were corrected to an equivalent dry basis using the laser absorption measured H_2O. The measured data shows agreement of the laser sensor with the GC measurements.

The operating conditions of Utah gasifier produced only a small amount of CH_4 (less than 1% of the syngas). However, gasifiers operating at lower temperature than the Utah facility or processing biomass instead of coal, produce much larger CH_4 mole fractions. Thus, it was useful to test the CH_4 measurements over a wider dynamic range, and controlled amounts of CH_4 were injected into the syngas flow sufficiently upstream of the measurement location to allow for uniform mixing with the product syngas. The variation of the CH_4 injection was made in discrete time-steps to facilitate understanding of the sensor time response, as captured by the sensor in Fig. 19.

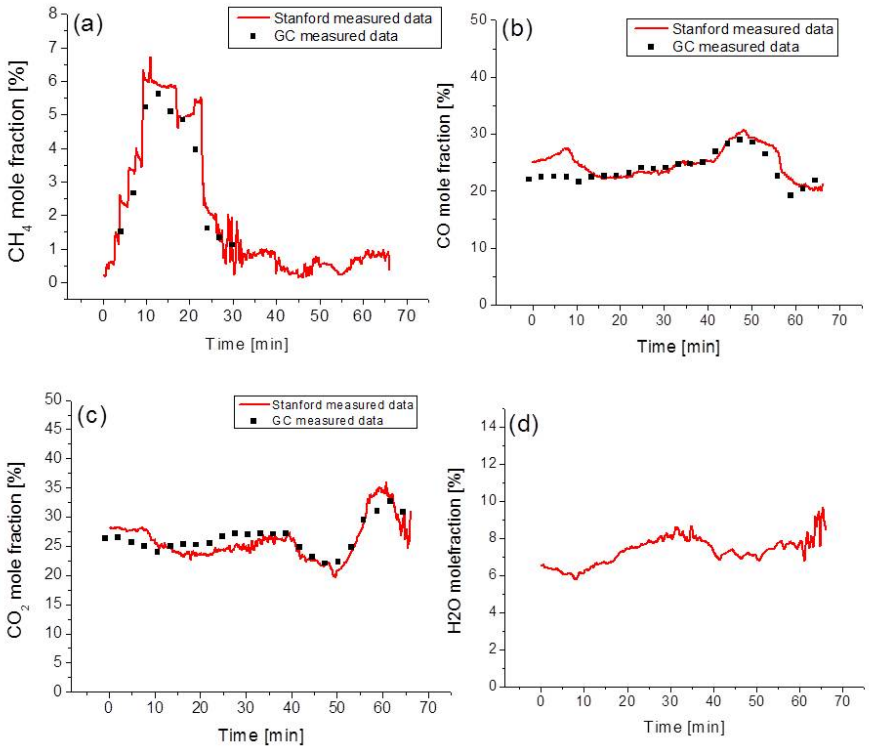

Figure 19. Time-resolved (dry basis except H_2O) laser absorption measured mole fractions of (a) CH_4, (b) CO, (c) CO_2 and (d) H_2O compared with GC measurements (except H_2O) in section 3 at 11 atm.

3.4 Summary of the Utah measurement campaigns

A prototype TDLAS-based syngas composition sensor was designed, constructed and tested in the laboratory at Stanford. This sensor was then optimized with a series of four field measurement campaigns to test performance in a pilot-scale gasifier at the University of Utah. During the fourth campaign, successful multi-species measurements of CO, CO_2, CH_4 and H_2O mole fractions were acquired in the gasifier at variety of operating conditions with a time resolution of ~3s. The absorption signals for the individual species were shown to be free of interference from other species by the measurement of 1*f*-normalized WMS-2*f* lineshape spectra. Reliable optical access to the poisonous, corrosive, high pressure and temperature syngas was developed and demonstrated. The major species composition of the syngas (for O_2-blown systems with significant but nearly constant amount of N_2) was determined from the measured CO, CO_2, H_2O, a separate monitor for N_2 (GC) and an assumption that the balance is H_2. When the important minor species CH_4 was included in the sensor suite, the energy content of the syngas could be determined within ± 5%. The LHV and Wobbe Index determined in the wet

syngas flow were in good agreement with dry values determined from gas sampling and GC analysis. The trends in the rise and fall of the CH_4, CO and CO_2 mole fractions correlate accurately with the physical changes in the gasifier after minimal time lag. Thus the prototype sensor demonstrated here has good promise for improved control of gasifier syngas quality.

4. Field measurements in an engineering-scale coal gasifier

Two field measurement campaigns to monitor the syngas output from the engineering-scale transport gasifier at the National Center for Carbon Capture (NCCC) in Wilsonville, AL were conducted. The first campaign tested the optical access and monitored H_2O during run R09 [26]. That measurement campaign was the first-ever *in situ* laser absorption in the syngas at the NCCC facility and a significant part of this first campaign involved developing a safe optical access for use in the commercial environment of the NCCC gasifier. The second campaign used the four species (CO, CO_2, CH_4, and H_2O) sensor refined in the Utah gasifier for measurements in the syngas during run R13 during March and April, 2014 [27]. The measurements were in good agreement with gas chromatography (GC) analysis of samples, but the *in situ* laser sensor had much faster time response, ~1 second compared with the 20 minute delay and 15 minute response of the GC analysis due to transit time and gas diffusion in the filters and driers in the sampling line. The time response of the *in situ* laser absorption and the rapid transport of the syngas products enabled gasifier reactor dynamics to be observed at the measurement location downstream of the particulate control device.

4.1 The gasifier at NCCC

The transport gasifier at NCCC is based on KBR's fluid catalytic cracking process [28, 29] and is illustrated in the photograph in Fig. 20 and the schematic of Fig. 21. Pulverized coal is added near the top of the mixing zone where the target temperature is 1260 K and air and steam are added at the bottom. The bed particles for this fluidized bed reactor are removed from the syngas in a pair of cyclones, the product stream cooled to ~600 K and most of the remaining particulate from the coal gasification removed by a proprietary particulate control device (PCD); the product syngas is specified to have 1 ppm solids by mass. The laser absorption measurement station for these measurements was located approximately 30 m further downstream as illustrated in Fig. 21, and the syngas conditions were approximately those listed in Table 5. The temperature at the flow exiting the transport reactor loop was monitored by a thermocouple and referred to here as the gasifier exit temperature (see Fig. 21).

Table 5 Typical conditions at the gasifier exhaust at NCCC

Temperature	600 K
Pressure	15 atm
Path length (pipe diameter)	20 cm
H_2O mole fraction	0.06 - 0.12
CO mole fraction	0.08 - 0.12
CO_2 mole fraction	0.06 - 0.10
H_2 mole fraction	0.06 - 0.10
CH_4 mole fraction	0.005 - 0.010
Trace species mole fraction (H_2S, NH_3, etc)	< 0.01
N_2 mole fraction	balance
Flow rate	Up to 12,500 kg/hr
Flow velocity at measurement location	10 -15 m/s

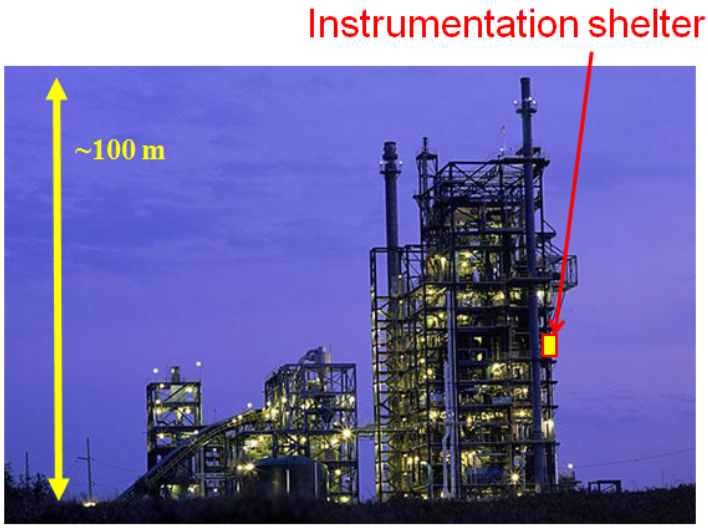

Figure 20. Photograph of the gasifier facility at NCCC.

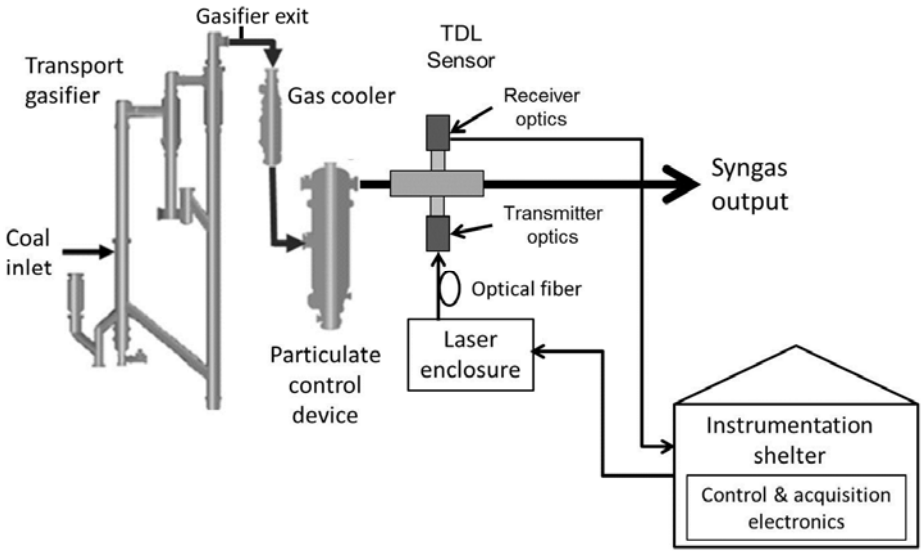

Figure 21. Schematic of the transport gasifier showing the location of the laser absorption station in the syngas output stream. Electronics were located approximately 30m away in an instrumentation shelter where ac power was allowed.

4.2 Optical engineering for installation of laser absorption sensor

The four-color, four-species laser absorption sensor used the optical access designed for the earlier H_2O measurements at NCCC [26]. The windows and the laser transmitter and receiver optics required for the line-of-sight absorption were mounted on opposing flanges on the syngas product duct as illustrated in Fig. 22. Redundant transmitter and receiver windows and shutoff ball valves provided isolation of the syngas flow in case of window failure. A pressure and temperature sensor mounted between each pair of windows would indicate fugitive syngas from a window leak, which was designed to trigger closure of the redundant ball valves to safely confine the syngas flow. The sapphire windows were 1" thick and were mounted onto 900lb ANSI flanges, which were pressure tested to 1600 psig at 400°F by the manufacturer. This

measurement location was on the fifth floor of the gasifier structure. Safety considerations limited the use of standard ac power to the instrumentation shelter shown in Fig. 22. Like the earlier campaign [26], the computer, data acquisition and the laser current and temperature controllers were housed in an instrument shelter approximately 30 m from the measurement station. However, the lasers were relocated from the instrumentation shelter to near the measurement station, and the transmitter and receiver heads were completely redesigned to enable four-species sensing with lasers outside the telecommunications band.

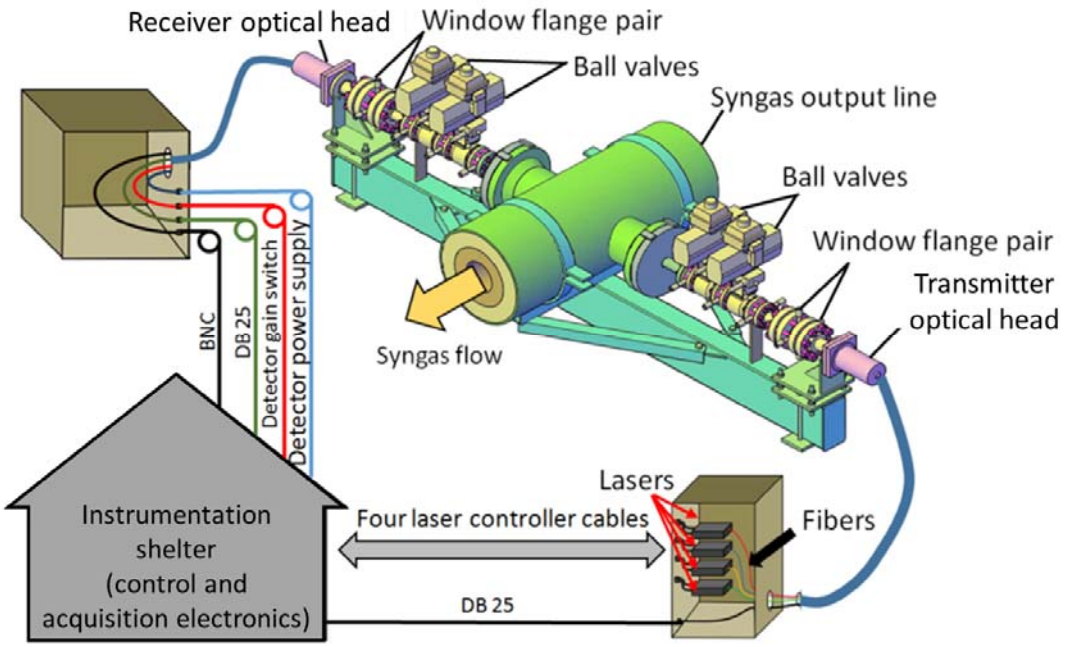

Figure 22. Schematic of the optical access and the laser absorption sensor in the syngas output flow channel; DB-25 provides optical alignment control signals.

The absorption transitions selected to optimize detection of CO, CO_2, and CH_4 are in the wavelength region 2-2.4 μm, which is beyond the useable range of telecommunications optical fiber. Thus, the lasers could not be located inside the instrumentation shelter and the light delivered to the transmitter head by fiber optics. Thus, the fiber lengths were limited to short (<2 m) distances with a minimum of fiber bending. The lasers were located in an explosion-proof, nitrogen-purged NEMA container about 1.5 m away from the transmitter optics. The purge served two purposes: (1) isolation of the electronics that may be considered an ignition hazard in case of fugitive syngas, and (2) heat transfer fluid to remove heat from the laser thermoelectric temperature control. Standard diode laser current and temperature controllers (ILX Lightwave LDC-3908) were located in the instrument shelter and connected via 30m shielded cables.

The four fiber-coupled lasers were multiplexed onto a single line-of-sight using a novel fiber bundle (Neptec Optical Solutions). Three extended NIR fibers (Thorlabs SM-2000, NA=0.11) for the CO, CO_2, and CH_4 lasers, and one telecommunications (Corning SMF-28+, NA=0.14) for the H_2O laser were bundled into a cable. The center-to-center separation of the four fiber cores was approximately 125μm, and the large NA rapidly overlaps the beams as they emerge from the end of fiber bundle, as illustrated in Fig. 23. The output was nearly collimated with a 75mm focal length plano-convex CaF_2 lens in the transmitter optics head and directed along the sensor

LOS. The diameters of the four beams were kept large to reduce the effect of beam steering. In the receiver optics head the four overlapped beams were collected with a 50 mm plano-convex CaF_2 lens and focused onto the 2mm x 2mm active area of a TE-cooled extended InGaAs detector (Hamamatsu).

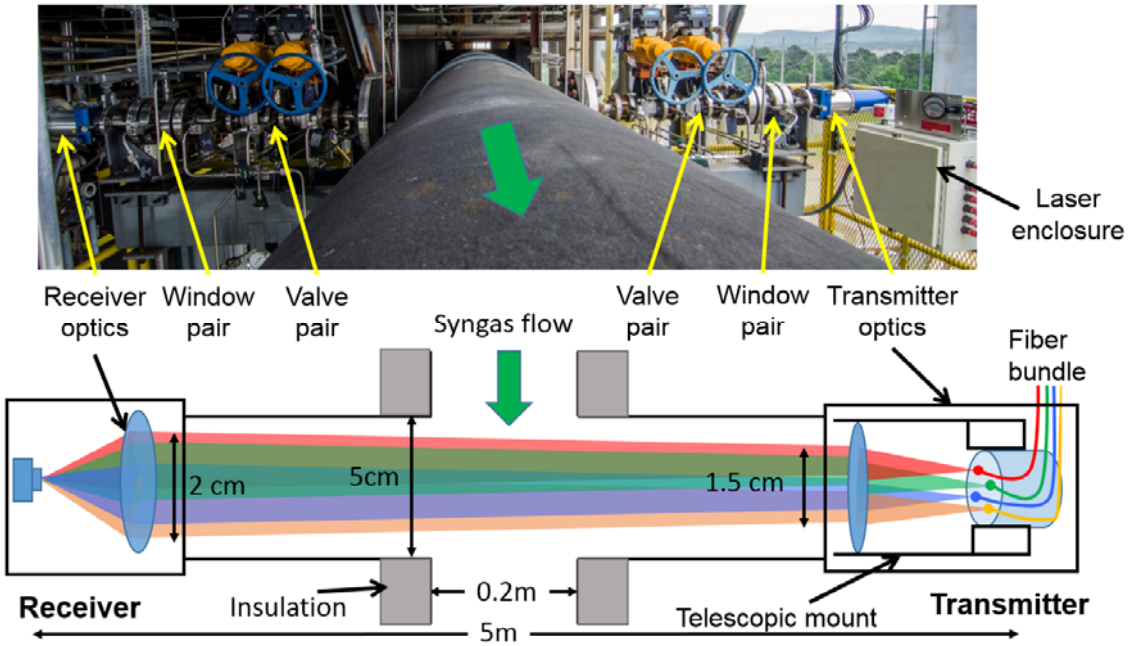

Figure 23. Multi-beam multiplexing hardware used for the four fiber-coupled NIR and extended NIR lasers.

Although remote angular adjustment could be done at any time from the control computer in the instrumentation house, the sensor alignment remained constant from optimization in the cold facility before their "leak-test cycle" until after gasifier shutdown, a period of 40 days.

4.3 Laser absorption measurements in the NCCC gasifier

During the 40 days of facility operation during the R13 campaign, time-resolved absorption data were collected for CO, CO_2, CH_4 and H_2O as the transport reactor transitioned through the following conditions:

1. Propane combustion to warm the internal ceramic linear of the gasifier
2. Pulsed-coal addition to the combustion in the second heating phase
3. Failed transitions from combustion to gasification
4. Successful transition to gasification
5. Pressure and temperature increase to target gasification conditions
6. Steady-state gasification
7. Reactor shut down at the end of the campaign

Laser absorption mole fraction measurements of CO, CO_2, and CH_4 were in good agreement with the facility gas chromatography (GC) analysis of sampled syngas. However, the sub-second time resolution of the laser absorption data revealed more dynamics in the syngas composition than the 15 minute time-constant observed for the GC analysis of sampled gas. Examples of the gasifier dynamics observed by the improved time resolution of the laser absorption measurements are shown below.

After the gasifier temperature stabilized at the target propane combustion pre-heat temperature, the fuel was transitioned from propane to pulsed-coal. These pulses provide an oscillating fuel/air equivalence ratio in the reactor that is captured by the time-resolved absorption measurements, as shown in Fig. 24. The ~2 minute period of these oscillations in combustion exhaust composition is too fast to be observed by the GC; however, the mean values of the GC CO_2 data agree with the laser absorption measurements to within 1% mole fraction.

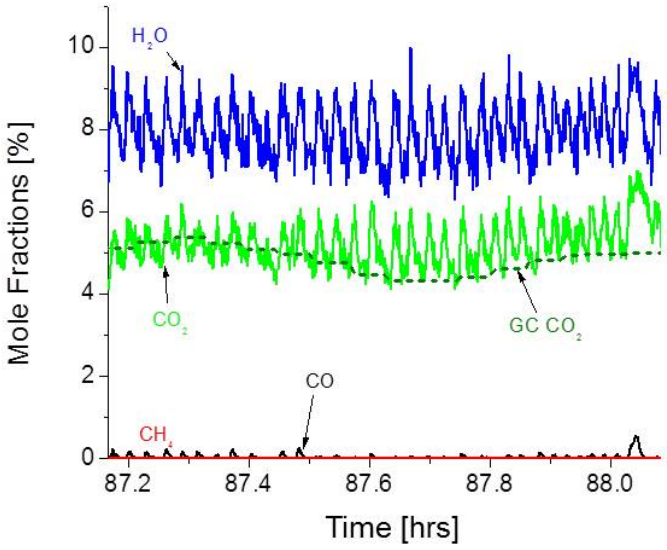

Figure 24. Pulsed fluctuations in CO, CO_2 and H_2O levels during initial parts of the coal-fed heat-up phase; data have 2.4 second time resolution compared with the GC measurements.

When the temperature in the reactor becomes hot enough to sustain coal oxidation, the propane flame is shut off, and reactor continues to heat from coal combustion. When the steady propane flame is turned off, the coal feed pulse rate is reduced, and the fluctuations in the gas composition become larger as seen in Fig. 25.

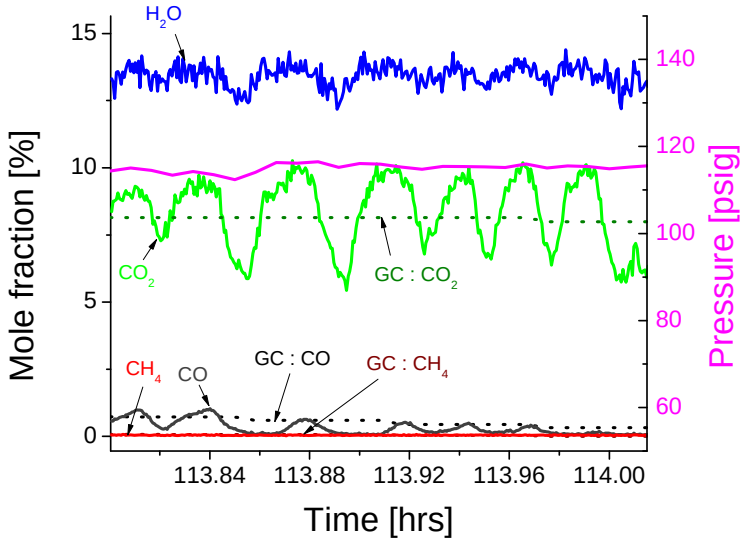

Figure 25. Pulsed fluctuations in laser absorption species concentration observed with 2.4 second resolution compared with GC measurements during the coal-fed heat-up phase.

At hour 121 of R13 the pressure had increased to 14 atm, the gasifier exit temperature to 1200 K, and the mixing zone temperature 1260 K. At this point an 840 hour (35 day) period of stable gasification was begun, and Fig. 26 shows the laser absorption measurements of mole fractions

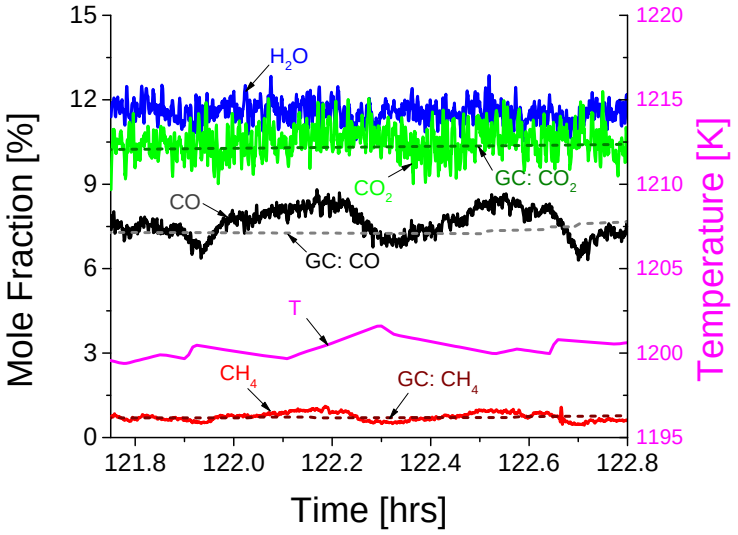

Figure 26. Laser sensor measurements of the four species, GC measurements of three species and gasifier exit temperature. Rapid oscillations track the coal batch feed, and slower oscillations in CO and CH_4 illustrate the stabilization of the reactor conditions.

of the four species at the beginning of this "steady-state" operation. First, we see rapid oscillation on mole fractions of all the species, which is superimposed on a slower variation. These variations were periodic with a ~23 minute period and were anti-correlated with the temperature variation as might be expected on examination of the water gas shift and methanation chemistry. Later in the operation, these slow oscillations cease and the data and the average mole fractions of all four species are remarkably constant and in excellent agreement with the GC as illustrated in Fig. 27. The mole fractions of all of the species in Fig. 27 have a pronounced oscillation with a period of approximately 13 minutes, which correlates with the oscillations in the gasifier exit temperature (also plotted). This correlation of the mole fractions with temperature show that small variations in the mixing zone conditions were not damped by diffusion after the ~5 second flow time to the laser absorption measurement station. Thus, even though the laser measurement was downstream of the transport gasifier reactor, the *in situ* measurements in the syngas flow offer the potential to track the reactor conditions.

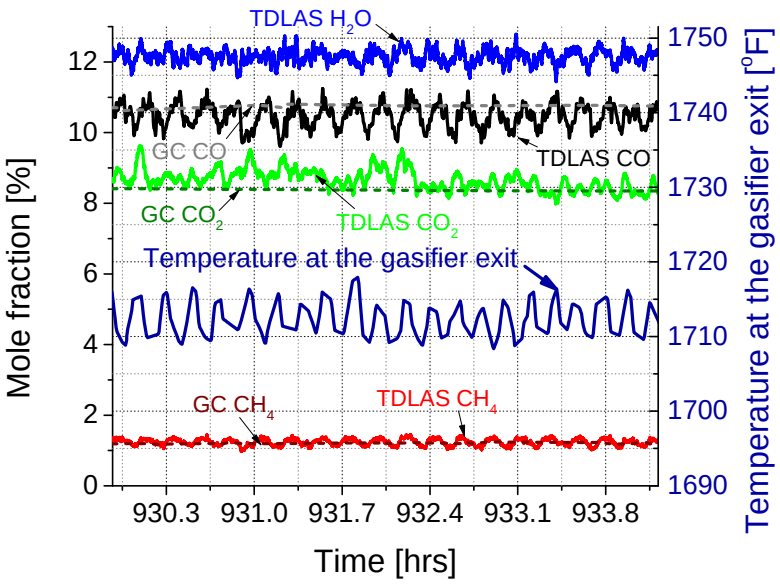

Figure 27. Time-resolved laser absorption data (2.4 second time resolution) track oscillations in the species mole fractions that are correlated with small changes in the gasifier exit temperature, which we speculate is due to the coal batch feed. Note the GC measurements of CH_4, CO_2, and CO do not capture these oscillations although the GC value is in good agreement with the average value of the laser absorption measurement.

Laser absorption and GC measurements are shown in Fig. 28 for the last four days of R13. The average laser absorption measurement of mole fraction is in good agreement with the GC values. The small rapid changes in gas composition observed in the laser data are not captured by the GC. Especially notable were the transients near 879 and 926 hours, which occurred due to blockage in the coal feed line, also seen in the GC measurements. Near 898 hours maintenance was performed on the GC to clear blockage in the gas sampling line, which was the only event in the entire 960 hour R13 campaign where the GC data indicated a transient not seen in the laser data, which suggests this is an artifact in the GC data set. At the end of the R13 run, there was a rapid transient as expected during the shutdown.

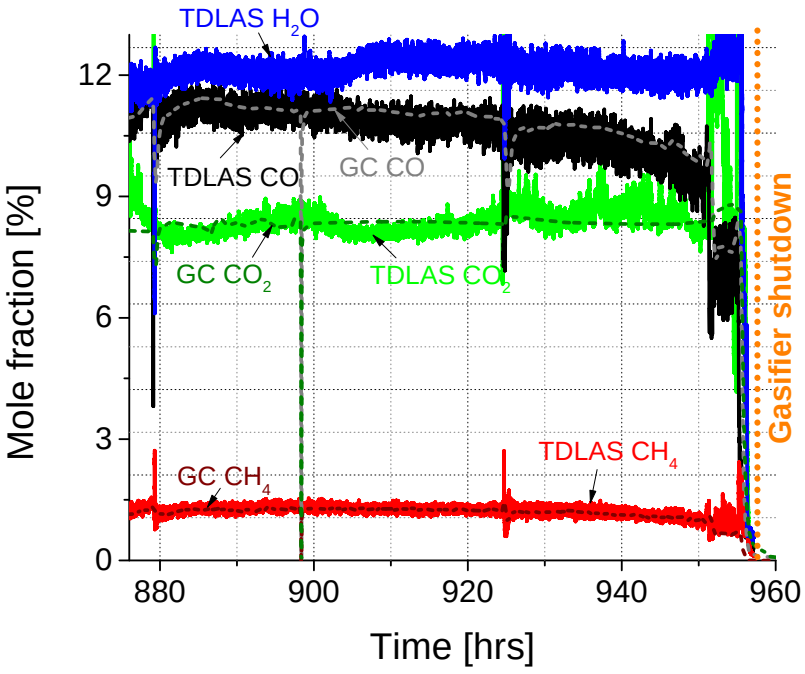

Figure 28. Laser absorption and GC measurement of mole fractions for the last four days of run R13 (220 psig and 630 K at the laser sensor location). At about 898 hrs, the GC sampling line was blocked and maintenance to clear the line produced a fast change in the GC reading at that time. The gasifier feed was unstable due to blockage in the coal feed line resulting in sharp changes in all the species concentrations at around 879 and 928 hrs.

4.4 Summary of the NCCC measurement campaigns

Time-division-multiplexed, *in-situ* wavelength-scanned 1*f*-normalized WMS-2*f* laser absorption measurements of CO, CO_2, CH_4, and H_2O mole fractions were demonstrated for the first time in an engineering-scale transport reactor gasifier. Single-sweep laser scanning provided a 20 millisecond time resolution, although the data presented here were averaged for one hundred wavelength scans of each laser (combined with computer and data storage overhead the laser data had 2.4 second time resolution). The measurements identified for the first time dynamic changes in the syngas composition that correlate with the fluctuations of the mixing zone temperature from the batch feeding of coal into the reactor. Such rapid laser absorption measurements of species mole fraction have the potential to optimize the batch feeding system. The rapid identifications in transient changes to the syngas composition show that the laser absorption sensor has excellent potential to guide the gasifier operator from startup to gasification. Once the gasifier has reached steady state operation, the sensor has the potential to rapidly identify problems (e.g., issues in batch feed of fuel) or to identify changes in the heating value of the fuel that might require adjustment of the gasifier tuning (air and steam addition). Significant optical engineering was required for safe optical windows to enable *in situ* measurements of the high-pressure and -temperature syngas. The use of a fiber bundle to combine onto a single absorption LOS the light from multiple lasers, whose wavelength range spanned more than 1μm, was especially novel.

5. Summary and conclusions

This project investigated the use of laser absorption sensing in particulate-laden syngas. Absorption transitions were selected with design rules to optimize signal strength while minimizing interference from other species. Successful *in situ* measurements in the dusty, high-pressure syngas flow were enabled by Stanford's normalized and scanned wavelength modulation strategy. A prototype sensor for CO, CH_4, CO_2, and H_2O was refined with experiments conducted in the laboratory at Stanford University, a pilot-scale at the University of Utah, and an engineering-scale gasifier at DoE's National Center for Carbon Capture. The demonstration measurement showed the *in situ* laser absorption sensor has the time response needed for reactor control. The NCCC measurement campaign demonstrated a technical readiness level of 6, and we anticipate only one more year of development would be needed to bring this multi-species laser absorption sensor for coal gasification (and other particulate-laden applications) to a technical readiness level of 7 or possibly 8; thus, we suggest this sensor presents an opportunity for future DoE investment.

6. References

1. S. J. Clayton, G. J. Stiegel, J. G. Wimer, *Gasification Technologies*: "Gasification Markets and Technologies – present and future: an industry perspective," DoE FE-0447 (2002).
2. L.S. Rothman et al., "The HITRAN2012 molecular spectroscopic database," *Journal of Quantitative Spectroscopy and Radiative Transfer*, vol. **130** (2013) 4-50.
3. M. P. Arroyo and R. K. Hanson, Appl. Opt. **32,** No. 30 (1993) 6104.
4. R. Sur, K. Sun, J.B. Jeffries, R.K. Hanson, "Design and testing of multi-species laser absorption sensors to monitor syngas composition," *Applied Physics B* **115** (2014) 9-24.
5. J. Reid and D. Labrie, "Second-harmonic Detection with tunable diode lasers-comparison of experiment and theory *Appl. Phys. B* **26** (1981) 203-210.
6. J.A. Silver, "Frequency-modulation spectroscopy for trace species detection: theory and comparison among experimental methods," *Appl. Opt.* **31** (1992) 707-717.
7. K. Uehara, H. Tai, "Remote detection of methane with a 1.66-μm diode laser," *Appl. Opt.* **31** (1992) 809–814.
8. L. C. Philippe, R. K. Hanson, "Laser diode wavelength-modulation spectroscopy for simultaneous measurement of temperature, pressure, and velocity in shock-heated oxygen flows," *Appl. Opt.* **32** (1993) 6090–6103.
9. R.K. Hanson, "Applications of quantitative laser sensors to kinetics, propulsion and practical energy systems*Proc. Combust. Inst.* **33** (2011) 1–40.
10. M.G. Allen, "Diode laser absorption sensors for gas dynamic and combustion flows," *Measurement Science and Technology* **9** (1998) 545-562.
11. P. Werle, "A review of recent advances in semiconductor laser based gas monitors," *Spectrochimica Acta Part A* **54** (1998) 197-236
12. J. Wolfrum, "Lasers in combustion: from basic theory to practical devices," *Proc. Combust. Inst.* **27** (1998) 1–41.
13. H. Li, G.B. Rieker, X. Liu, J.B. Jeffries, R.K. Hanson, "Extension of wavelength-modulation spectroscopy to large modulation depth for diode laser absorption measurements in high-pressure gases," *Appl. Opt.* **45** (2006) 1052-1061.
14. D.T. Cassidy, J. Reid, "Atmospheric pressure monitoring of trace gases using tunable diode lasers," *Appl. Opt* **21** (1982) 1185-1190.

15. T. Fernholz, H. Teichert, V. Ebert, "Digital, Phase-Sensitive Detection for *In Situ* Diode Laser Spectroscopy under Rapidly Changing Transmission Conditions," *Appl. Phys. B* **75** (2002) 229–236.
16. K. Uehara, H. Tai, "Remote detection of methane with a 1.66-μm diode laser," *Appl. Opt.* **31** (2002) 809–814
17. G.B. Rieker, J.B. Jeffries, R.K. Hanson, "Calibration-free wavelength-modulation spectroscopy for measurements of gas temperature and concentration in harsh environments," *Appl. Opt.* **48** (2009) 5546-5560.
18. K. Sun, R. Sur, X.Chao, J.B. Jeffries, R.K. Hanson, R.J. Pummill, K.J. Whitty, TDL absorption sensors for gas temperature and concentrations in a high-pressure entrained-flow coal gasifier," *Proc. Combustion Institute* **34** (2013) 3593-3601.
19. K. Sun, R. Sur, X. Chao, J.B. Jeffries, R.K. Hanson, R.J. Pummill, D.A. Wagner, K. J. Whitty, R.C. Steele, "Temperature measurements in an entrained-flow, slagging, coal gasifier using laser absorption of water vapor, *Pittsburgh Coal Conference*, (2011).
20. I.A. Schultz, C.S. Goldenstein, J.B. Jeffries, R.K. Hanson, R.D. Rockwell, C.P. Goyne, "Spatially-resolved water measurements in a scramjet combustor using diode laser absorption," *Journal of Propulsion and Power* (also AIAA, 2014-1241), (2014) doi. 1-8, 10.2514/1.B35219.
21. K. Sun, X. Chao, C.S. Goldenstein, R. Sur, J.B. Jeffries, R.K. Hanson, "Analysis of calibration-free wavelength-scanned-wavelength-modulation spectroscopy for practical gas sensors using tunable diode lasers," *Measurement Science and Technology* **24** (2013) 125203 doi:10.1088/0957-0233/24/12/125203.
22. C.S. Goldenstein, C.L. Strand, I. A. Schultz, K. Sun, J. B. Jeffries, R.K. Hanson, "Fitting of calibration-free scanned-wavelength-modulation spectroscopy spectra for determination of gas properties and absorption lineshapes," *Applied Optics* **53** (2014) 356-367.
23. J. Humlicek, J. Quant. Spectrosc. Radiat. Transfer **27**, No. 4, (1982) 437.
24. M.W. Chase Jr., JANAF-NIST Thermochemical Tables, J. Phys. and Chem. Ref. data: Monograph No. **9** (1998).
25. R. Sur, K. Sun, J.B. Jeffries, R.K. Hanson, R.J. Pummill, T. Waind, D.R. Wagner, and K. Whitty, "TDLAS-based sensors for *in situ* measurement of syngas composition in a pressurized, oxygen-blown, entrained-flow coal gasifier," Applied Physics B, (2014), online first, DOI 10.1007/s00340-013-5644-6.
26. K. Sun, R. Sur, J.B. Jeffries, R.K. Hanson, T. Clark, J. Anthony, S. Machovec, J. Northington, "Application of wavelength-scanned WMS H_2O absorption measurements in an engineering-scale high-pressure coal gasifier," Applied Physics B *B* **117** (2014) 411-421, DOI: 10.1007/s00340-014-5850-x.
27. R. Sur, K. Sun, J.B. Jeffries, J.G. Socha, R.K. Hanson, "Scanned-wavelength-modulation-spectroscopy sensor for CO, CO_2, CH_4, and H_2O in a high-pressure engineering-scale transport-reactor coal-gasifier," *Fuel*, submitted 2014.
28. S. Ariyapadi, P. Shires, M. Bhargava, and D. Ebbern, "KBR's Transport Gasifier (TRIG^{TM}) – An Advanced Gasification Technology for SNG Production from Low-Rank Coals," in *Twenty-Fifth Annual International Pittsburgh Coal Conference* (2008).
29. J. M. Wheeldon, *National Carbon Capture Center: 2010 Report* (2010).

Publications

The results of this research grant have been published in seven peer reviewed manuscripts, one patent, eleven conference presentations, and three PhD theses.

1. Articles in peer reviewed journals

1. K. Sun, R. Sur, X.Chao, J.B. Jeffries, R.K. Hanson, R.J. Pummill, K.J. Whitty, TDL absorption sensors for gas temperature and concentrations in a high-pressure entrained-flow coal gasifier," *Proc. Combustion Institute* **34** (2013) 3593-3601.
2. K. Sun, X. Chao, R. Sur, J.B. Jeffries, R.K. Hanson, "Wavelength modulation diode laser absorption spectroscopy for high pressure gas sensing," *Applied Physics B* **110** (2013) 497-508.
3. R. Sur, K. Sun, J.B. Jeffries, R.K. Hanson, "Design and testing of multi-species laser absorption sensors to monitor syngas composition," *Applied Physics B* **115** (2014) 9-24.
4. R. Sur, K. Sun, J.B. Jeffries, R.K. Hanson, R.J. Pummill, T. Waind, D.R. Wagner, and K. Whitty, "TDLAS-based sensors for *in situ* measurement of syngas composition in a pressurized, oxygen-blown, entrained-flow coal gasifier," Applied Physics B, (2014), online first, DOI 10.1007/s00340-013-5644-6.
5. K. Sun, X. Chao, C.S. Goldenstein, R. Sur, J.B. Jeffries, R.K. Hanson, "Analysis of calibration-free wavelength-scanned-wavelength-modulation spectroscopy for practical gas sensors using tunable diode lasers," *Measurement Science and Technology,* Technology 24 (2013) 125203 doi:10.1088/0957-0233/24/12/125203 (selected paper of the year by the journal).
6. K. Sun, R. Sur, J.B. Jeffries, R.K. Hanson, T. Clark, J. Anthony, S. Machovec, J. Northington, "Application of wavelength-scanned WMS H_2O absorption measurements in an engineering-scale high-pressure coal gasifier," Applied Physics B *B* **117** (2014) 411-421, DOI: 10.1007/s00340-014-5850-x.
7. R. Sur, K. Sun, J.B. Jeffries, J.G. Socha, R.K. Hanson, "Scanned-wavelength-modulation-spectroscopy sensor for CO, CO_2, CH_4, and H_2O in a high-pressure engineering-scale transport-reactor coal-gasifier," *Fuel*, submitted 2014.

2. Patent

A Method for Calibration-Free Scanned-Wavelength Modulation Spectroscopy for Gas Sensing, Stanford Docket Number 11-4-3, 14/367,420 (USA pending) filed 6/20/2014 and 201280070094.9 (China pending) filed 12/19/2012

3. Conference presentations

1. K.J. Whitty, R.J. Pummill, T. Waind, D.A. Wagner, D.R. Wagner, "Performance of a 500 kWth pressurized entrained flow coal gasifier," *Pittsburgh Coal Conference*, Istanbul, Turkey (2010).
2. R.J. Pummill, K.J. Whitty, "Predicting slag behavior in an entrained flow gasifier: A two-dimensional analysis of slag flow," *Pittsburgh Coal Conference*, Istanbul, Turkey (2010).
3. K. Sun, R. Sur, J.B. Jeffries, R.K Hanson, R.J. Pummill, D.A. Wagner, K.J. Whitty, "Diode laser absorption measurements in an entrained-flow, slagging, coal gasifier," *7th US National Meeting of the Combustion Institute*, Atlanta, GA (2011).

4. K. Sun, R. Sur, X. Chao, J.B. Jeffries, R.K. Hanson, R.J. Pummill, D.A. Wagner, K. J. Whitty, R.C. Steele, "Temperature measurements in an entrained-flow, slagging, coal gasifier using laser absorption of water vapor, *Pittsburgh Coal Conference*, (2011).
5. K.J. Whitty, "Acquisition and analysis of data in a pressurized entrained-flow coal gasifier for the purposes of simulation validation," *NETL 2011 Workshop on Multiphase Flow Science,* Pittsburgh, PA (2011).
6. K. Sun, R. Sur, X.Chao, J.B. Jeffries, R.K. Hanson, R.J. Pummill, K.J. Whitty, TDL absorption sensors for gas temperature and concentrations in a high-pressure entrained-flow coal gasifier," *34th International Combustion Symposium*, Warsaw, Poland, July, 2012.
7. J.B. Jeffries, R.K. Hanson, K.J. Whitty, "Tunable Diode Laser Sensors for Monitoring Combustion and Gasification Systems," DoE-EPRI Workshop on Instrumentation, Austin, TX, June, 2012.
8. R. Sur, K. Sun, J.B. Jeffries, R.K. Hanson, R.S. Pummill and K.J. Whitty, "TDLAS-based *in situ* monitoring of syngas composition from an oxygen-blown, down-fired coal gasifier," 8th US National Comb. Meeting, Park City, UT, May, 2013.
9. K. Sun, R. Sur, J.B. Jeffries, R.K. Hanson, T. Clark, J. Anthony, S. Machovec and J. Northington, "*In situ* measurements of syngas temperature, water vapor and carbon dioxide in an engineering-scale, fluidized-bed coal gasifier," 8th US National Comb. Meeting, Park City, UT, May, 2013.
10. K.J. Whitty, R.S. Pummill, R. Sur, K. Sun, J.B. Jeffries, R.K. Hanson, "Demonstration of Tunable Diode Laser-Based In-Situ Monitoring of Syngas Composition for Pressurized Entrained-Flow Coal Gasification," Gasification Technologies Conference, Colorado Springs, CO, October, 2013.
11. J.B. Jeffries, R. Sur, K. Sun, R.K. Hanson, "Laser-absorption sensing of gas composition of products from coal gasification," SPIE DSS Conference: Micro- and Nanotechnology Sensors, Systems, and Applications VI, vol. 9083, paper 28, May, 2014.

4. PhD theses

1. R.J. Pummill, "*Physical and Computational Studies of Slag Behavior in an Entrained Flow Gasifier*," PhD Dissertation, Dept. of Chemical Engineering, The University of Utah, Salt Lake City, UT, June, 2012.
2. K. Sun, "*Utilization of multiple harmonics of wavelength modulation absorption spectroscopy for practical-gas sensing*," PhD Dissertation, Stanford University, Department of Mechanical Engineering, Stanford, CA, December, 2013, http://hanson.stanford.edu/dissertations/Sun_2013.pdf.
3. R. Sur, "*Development of robust TDLAS sensors for combustion products at high pressure and temperature in energy systems,*" PhD Dissertation, Stanford University, Department of Mechanical Engineering, Stanford, CA, December, 2014.